



## Abstract

Anthropogenic aerosol effects on climate produce one of the largest uncertainties in estimates of radiative forcing of past and future climate change. Much of this uncertainty arises from the multi-scale nature of the interactions between aerosols, clouds and large-scale dynamics, which are difficult to represent in conventional global climate models (GCMs). In this study, we develop a multi-scale aerosol climate model that treats aerosols and clouds across different scales, and evaluate the model performance, with a focus on aerosol treatment. This new model is an extension of a multi-scale modeling framework (MMF) model that embeds a cloud-resolving model (CRM) within each grid column of a GCM. In this extension, the effects of clouds on aerosols are treated by using an explicit-cloud parameterized-pollutant (ECPP) approach that links aerosol and chemical processes on the large-scale grid with statistics of cloud properties and processes resolved by the CRM. A two-moment cloud microphysics scheme replaces the simple bulk microphysics scheme in the CRM, and a modal aerosol treatment is included in the GCM. With these extensions, this multi-scale aerosol-climate model allows the explicit simulation of aerosol and chemical processes in both stratiform and convective clouds on a global scale.

Simulated aerosol budgets in this new model are in the ranges of other model studies. Simulated gas and aerosol concentrations are in reasonable agreement with observations, although the model underestimates black carbon concentrations at the surface. Simulated aerosol size distributions are in reasonable agreement with observations in the marine boundary layer and in the free troposphere, while the model underestimates the accumulation mode number concentrations near the surface, and overestimates the accumulation number concentrations in the free troposphere. Simulated cloud condensation nuclei (CCN) concentrations are within the observational variations. Simulated aerosol optical depth (AOD) and single scattering albedo (SSA) are in reasonable agreement with observations, and the spatial distribution of AOD is consistent with observations, while the model underestimates AOD over regions with

# GMDD

3, 1625–1695, 2010

## A multi-scale aerosol climate model

M. Wang et al.

[Title Page](#)

[Abstract](#)

[Introduction](#)

[Conclusions](#)

[References](#)

[Tables](#)

[Figures](#)

[I◀](#)

[▶I](#)

[◀](#)

[▶](#)

[Back](#)

[Close](#)

[Full Screen / Esc](#)

[Printer-friendly Version](#)

[Interactive Discussion](#)



strong fossil fuel and biomass burning emissions, and overestimates AOD over regions with strong dust emissions. Overall, this multi-scale aerosol climate model simulates aerosol fields as well as conventional aerosol models.

## 1 Introduction

5 Atmospheric aerosols are an important component of the global climate system. They can affect the climate system directly by scattering or absorbing solar radiation, and indirectly through their effects on clouds by acting as cloud condensation nuclei (CCN) or ice nuclei (IN). However, despite more than a decade of active research, anthropogenic aerosol effects on climate still produce one of the largest uncertainties in the  
10 estimates of radiative forcing of past and future climate change (IPCC, 2007).

Much of this uncertainty arises from the multi-scale nature of the interactions between aerosols, clouds and large-scale dynamics, which are difficult to represent in conventional global climate models (GCMs). These interactions span a wide range in spatial scales, from 0.01–1000  $\mu\text{m}$  for droplet and crystal nucleation, aqueous-phase  
15 chemistry, precipitation, and collection, to 100–1000 m for marine stratus, to 1–2 km for shallow cumulus, to 2–10 km for deep convection, and to 50–100 km for large scale cloud systems. Given the typical GCM grid spacing of 100–400 km, the treatment of most of those processes in conventional GCMs is highly parameterized and, therefore, also highly uncertain.

20 Representing aerosol/cloud processes in deep cumulus has been most problematic in global climate models. Cumulus parameterizations in current climate models rely on ad hoc closure assumptions designed to diagnose the latent heating and vertical transport of heat and moisture by deep convection, and provide little information about microphysics or updraft velocity (Del Genio et al., 2005; Emanuel and Zivkovic-  
25 Rothman, 1999; Zhang et al., 2005). As a result, aerosol effects on cumulus clouds are only represented, sometimes crudely, in a handful of GCMs using cumulus parameterizations (Lohmann, 2008; Menon and Rotstayn, 2006; Nober et al., 2003). Meanwhile,

## A multi-scale aerosol climate model

M. Wang et al.

[Title Page](#)

[Abstract](#)

[Introduction](#)

[Conclusions](#)

[References](#)

[Tables](#)

[Figures](#)

[◀](#)

[▶](#)

[◀](#)

[▶](#)

[Back](#)

[Close](#)

[Full Screen / Esc](#)

[Printer-friendly Version](#)

[Interactive Discussion](#)



field and satellite measurements and simulations by cloud-resolving models (CRMs) provide increasing evidence that aerosols influence cumulus clouds (Andreae et al., 2004; Cui et al., 2006; Koren et al., 2004, 2005; Rosenfeld et al., 2008; Wang, 2005).

In addition, cumulus clouds play critical roles in determining the vertical distributions and lifetime of most aerosols. Convective clouds are responsible for much of the vertical transport of pollutants, the aqueous chemistry, and the removal of pollutants from the atmosphere (Chatfield and Crutzen, 1984; Ekman et al., 2006; Wang and Prinn, 2000). Easter et al. (2004) showed that convective clouds account for 80–95% of accumulation-mode aerosol number removal, 65–85% of carbonaceous aerosol wet removal, 50–85% of sulfate wet removal, and 10–70% of in-cloud SO<sub>2</sub> oxidation in their global aerosol climate model. However, the treatment of convective cloud processes in global aerosol models is based on cumulus parameterizations, which are highly uncertain (Bechtold et al., 2000; Xie et al., 2002; Xu et al., 2002; Gregory and Guichard, 2002). In the global aerosol climate model used by Easter et al. (2004), the large range (10–70%) for in-cloud SO<sub>2</sub> oxidation reflects different assumptions made about the cloud volume of convective clouds, which is generally not predicted by cumulus parameterizations. Simulated vertical distributions of gas and aerosol species in global models have been shown to largely depend on the convective parameterization (Iversen and Seland, 2002; Jacob et al., 1997; Mahowald et al., 1995; Rasch et al., 2000).

To avoid the problems in cumulus parameterizations in GCMs, Suzuki et al. (2008) simulated aerosol-cloud interactions in convective clouds on global scale by using an aerosol-coupled global CRM with a horizontal grid spacing of 7 km. They showed that the model realistically simulated detailed spatial structure of cloud droplet effective radii and the relationship between liquid water path and aerosol optical properties, compared with satellite data. However, Suzuki's model is extremely expensive and hence was only run for 7 days. Given the high computational cost, it will not be feasible to use global CRMs with online aerosols for long-term climate-relevant simulations (decades) for at least five years and probably longer.

**A multi-scale aerosol climate model**

M. Wang et al.

[Title Page](#)[Abstract](#)[Introduction](#)[Conclusions](#)[References](#)[Tables](#)[Figures](#)[◀](#)[▶](#)[◀](#)[▶](#)[Back](#)[Close](#)[Full Screen / Esc](#)[Printer-friendly Version](#)[Interactive Discussion](#)

**A multi-scale aerosol climate model**

M. Wang et al.

[Title Page](#)[Abstract](#)[Introduction](#)[Conclusions](#)[References](#)[Tables](#)[Figures](#)[◀](#)[▶](#)[◀](#)[▶](#)[Back](#)[Close](#)[Full Screen / Esc](#)[Printer-friendly Version](#)[Interactive Discussion](#)

A new type of global climate model called the multi-scale modeling framework (MMF) model, first introduced a decade ago (Grabowski, 2001; Khairoutdinov and Randall, 2001), uses a cloud resolving model (CRM) at each grid column of a host GCM to replace conventional parameterizations for moist convection and large scale condensation. This approach permits explicit simulations of deep convective clouds for the whole global domain, while keeping the computational cost acceptable for multi-year climate simulations. The subgrid variability in cloud dynamics and cloud microphysics is explicitly resolved at spatial scales down to the resolution of the CRM. The MMF models have been shown to improve climate simulations in several important ways (Ovtchinnikov et al., 2006; Pritchard and Somerville, 2009a, b; Khairoutdinov et al., 2008; Tao et al., 2009).

The MMF model would be an ideal tool to study aerosol effects on climate on global scale given its multi-scale nature and its moderate computational cost compared with global CRMs. However, several limitations in the original MMF (Khairoutdinov et al., 2008) have hindered its usage in studying aerosol effects on climate. First, the original MMF did not include any treatment of aerosol and chemical processes. Second, the original MMF has an oversimplified microphysics treatment consisting of only two predicted water variables. This simple scheme neglected the complex interactions between different hydrometers and did not represent a variety of processes (e.g., the Bergeron-Findeisen process, droplet activation, and ice nucleation) that are important to the study of aerosol-cloud interactions.

In this study, we address these challenges and extended the original MMF in the following ways. First, the host GCM model is updated to use a modal aerosol approach to treat aerosol processes and represent aerosol size distributions; second, an explicit-cloud parameterized-pollutant (ECP) approach (Gustafson et al., 2008) is added to link aerosol and chemical processes on the GCM grid with statistics of cloud properties resolved by the CRM, and third, a two-moment cloud microphysics scheme replaces the simple one moment scheme in the CRM. With these changes, the new MMF model (Pacific Northwest National Laboratory MMF, or PNNL-MMF) has the capability to study

aerosol-cloud interactions from cumulus to global scales. In this paper, we have documented these changes, with a focus on aerosol and chemical treatment, and evaluate the model results. Section 2 documents the improvements in detail, and the model results are shown in Sects. 3 and 4. Finally, Sect. 5 is the summary.

## 2 Model description and set-up of simulations

The PNNL-MMF is an extension of the Colorado State University (CSU) MMF model (Khairoutdinov et al., 2005, 2008), first developed by Khairoutdinov and Randall (2001). The CSU MMF was based on the Community Atmospheric Model (CAM) version 3.5, which is the atmospheric component of the NCAR Community Climate System Model (Collins et al., 2006). The embedded CRM in each GCM grid column is a two-dimensional version of the System for Atmospheric Modeling (SAM) (Khairoutdinov and Randall, 2003), which replaces the conventional moist physics, convective, turbulence, and boundary layer parameterizations, except for the gravity wave drag parameterization in CAM. During each GCM time step (every 10 min), the CRM is forced by the large-scale temperature and moisture tendencies arising from GCM-scale dynamical process and feeds the response back to the GCM-scale as heating and moistening terms in the large-scale budget equations for heat and moisture. The CRM runs continuously using a 20-s time step. The CAM radiative transfer code is applied to each CRM column at every GCM time step (10 min), assuming 1 or 0 cloud fraction at each CRM grid point, which eliminates the cloud overlap assumptions used in conventional GCMs.

In this study, both the GCM and CRM components are updated from what is used in the CSU MMF. A third component, the ECPP approach, is added to link aerosol and chemical processes on the GCM grids with statistics of cloud properties resolved by the CRM. Those extensions in the PNNL-MMF are documented in detail below.

## A multi-scale aerosol climate model

M. Wang et al.

Title Page

Abstract

Introduction

Conclusions

References

Tables

Figures



Back

Close

Full Screen / Esc

Printer-friendly Version

Interactive Discussion



## 2.1 The NCAR CAM5 atmospheric GCM

The host GCM in the PNNL MMF has been updated to version five of CAM (CAM5). Although CAM5 differs from CAM3.5 in many respects (e.g., cloud microphysics, cloud macrophysics, turbulence, shallow cumulus, aerosols, and radiative transfer), most of the changes are not relevant to the MMF model since the treatments of clouds and turbulence are replaced with the treatments in the CRM. The differences that are relevant to the MMF model are in the treatment of radiative transfer and of the aerosol lifecycle, which are briefly described below.

The radiative transfer scheme in CAM5 is the Rapid Radiative Transfer Model for GCMs (RRTMG), a broadband k-distribution radiation model developed for application to GCMs (Iacono et al., 2003, 2008; Mlawer et al., 1997).

A modal approach is used to treat aerosols in CAM5 (Liu et al., 2010). Aerosol size distributions are represented by using three or seven log-normal modes. The three-mode version adopted in this study has been shown to simulate aerosol fields in reasonable agreement with the 7-mode treatment and is computationally more efficient, which makes it more suitable for long-term climate simulations (Liu et al., 2010). The three-mode version has an Aitken mode, an accumulation mode, and a single coarse mode. Aitken mode species include sulfate, secondary organic carbon (SOA), and sea salt; accumulation mode species include sulfate, SOA, black carbon (BC), primary organic carbon (POM), sea salt, and dust; coarse mode species include sulfate, sea salt, and dust. Species mass and number mixing ratios are predicted for each mode, while mode widths are prescribed. Both aerosols outside the cloud droplets (interstitial) and aerosols in the cloud droplets (cloud-borne) are predicted. Aerosol nucleation from  $\text{H}_2\text{SO}_4$ , condensation of trace gases ( $\text{H}_2\text{SO}_4$ , and semi-volatile organics) on existing aerosol particles, and coagulation (Aitken and accumulation modes) are treated. Water uptake and optical properties for each mode are expressed in terms of both relative humidity (accounting for hysteresis) and the hygroscopicities of the mode's component. The model simulates DMS,  $\text{SO}_2$ ,  $\text{H}_2\text{SO}_4$ ,  $\text{H}_2\text{O}_2$ , and SOA gases, using monthly

# GMDD

3, 1625–1695, 2010

## A multi-scale aerosol climate model

M. Wang et al.

[Title Page](#)

[Abstract](#)

[Introduction](#)

[Conclusions](#)

[References](#)

[Tables](#)

[Figures](#)

[◀](#)

[▶](#)

[◀](#)

[▶](#)

[Back](#)

[Close](#)

[Full Screen / Esc](#)

[Printer-friendly Version](#)

[Interactive Discussion](#)



averaged oxidant fields (OH, O<sub>3</sub>, and NO<sub>3</sub>) produced by a version of CAM with detailed gas-phase chemistry.

In the standard CAM5, cloud fields from the conventional cloud parameterizations are used to drive the convective transport, aerosol activation in stratiform clouds, aqueous chemistry, and wet scavenging for aerosol and gas species. In the PNNL-MMF, the treatment of cloud-related aerosol and gas processes (i.e., aqueous chemistry, convective transport, and wet scavenging) in the standard CAM5 is replaced by the ECPP approach (Sect. 2.3), which uses cloud statistics simulated by the CRM to drive the aerosol processing by clouds.

## 2.2 The SAM CRM

The original SAM used in the CSU MMF had a simple bulk microphysics scheme in which only the liquid/ice-water moist static energy, the total nonprecipitating water, and the total precipitating water were predicted (Khairoutdinov and Randall, 2003). The mixing ratio of cloud water, cloud ice, rain, snow and graupel were diagnosed from the prognostic variables using temperature-dependent partitioning between liquid and ice. This simple scheme neglected the complex interactions between different hydrometers and was not able to represent a variety of processes (e.g., the Bergeron-Findeisen process, droplet activation, and ice nucleation) that are important to the study of aerosol-cloud interactions.

In the PNNL-MMF, a double-moment microphysics scheme from Morrison et al. (2005, 2009) replaces the simple bulk microphysics in the CRM model. The new scheme predicts the number concentrations and mixing ratios of five hydrometer types (cloud droplets, ice crystals, rain, snow, and graupel). The precipitation hydrometer types (rain, snow, and graupel) are fully prognostic in the CRM model, rather than diagnostic as in CAM5. Droplet activation from hydrophilic aerosols, ice nucleation, ice crystal growth by vapor deposition, the dependence of ice crystal sedimentation on crystal number, and the dependence of autoconversion on droplet number are treated, in addition to several other microphysical processes.

## A multi-scale aerosol climate model

M. Wang et al.

[Title Page](#)

[Abstract](#)

[Introduction](#)

[Conclusions](#)

[References](#)

[Tables](#)

[Figures](#)

[⏪](#)

[⏩](#)

[◀](#)

[▶](#)

[Back](#)

[Close](#)

[Full Screen / Esc](#)

[Printer-friendly Version](#)

[Interactive Discussion](#)



Droplet activations are calculated at each CRM grid point, based on the parameterization of Abdul-Razzak and Ghan (2000). The vertical velocity used in droplet activation is the sum of the vertical velocity resolved at the CRM grid point and a sub-grid vertical velocity ( $\sigma_{\text{crmw}}$ ) that accounts for the unresolved motion. The subgrid vertical

velocity is diagnosed from the turbulent kinetic energy (TKE):  $\sigma_{\text{crmw}} = \sqrt{(\text{TKE}/3)}$ , where the TKE is predicted or diagnosed in the SAM CRM, depending on its sub-grid model. A simple Smagorinsky-type scheme is used to treat the subgrid-scale fluxes in the SAM model, and the TKE is diagnosed from the eddy viscosity. A minimum vertical velocity of  $0.1 \text{ m s}^{-1}$  is set for calculating droplet activation. Aerosol fields used in droplet activation in the CRM are predicted on the GCM grid cells by CAM5, in which cloud-related aerosol processes are treated by using the ECPP approach (Sect. 2.3).

The CAM radiative transfer scheme (RRTMG) is applied to each CRM column, assuming 1 or 0 cloud fraction at each CRM grid point. Aerosol water uptake is calculated at each CRM grid point, which accounts for the subgrid variation in relative humidity within each GCM grid cell. Aerosol water at the CRM grids together with dry aerosol on the GCM grids are used to calculate aerosol optical properties at each CRM grid.

### 2.3 The Explicit-Cloud-Parameterized-Pollutant (ECPP) approach

As we discussed in the introduction, one of the limitations in the CSU MMF is its lack of treatment of aerosol and chemical processes. An ideal way to account for these processes in the MMF model would be to add their treatment into the CRM component, thereby simulating aerosol and chemical processes directly on cloud scales. Given the large number of species and numerous processes involved, however, this approach is not computationally feasible for multi-year climate simulations in the near future. In this study, we take an alternative approach, the Explicit-Cloud Parameterized-Pollutant method (ECPP) (Gustafson et al., 2008). The ECPP approach uses statistics of cloud properties resolved by the CRM (Explicit-Cloud) to drive aerosol and chemical processing by clouds on the GCM grids (Parameterized-Pollutant), which allows us to explicitly

## A multi-scale aerosol climate model

M. Wang et al.

[Title Page](#)

[Abstract](#)

[Introduction](#)

[Conclusions](#)

[References](#)

[Tables](#)

[Figures](#)

[◀](#)

[▶](#)

[◀](#)

[▶](#)

[Back](#)

[Close](#)

[Full Screen / Esc](#)

[Printer-friendly Version](#)

[Interactive Discussion](#)



account for the effects of convective clouds on aerosols while being computationally feasible. The treatment of vertical transport of tracers within ECPP is documented in detail in Gustafson et al. (2008) and is slightly modified in this study. The ECPP treatment is also extended to treat aerosol activation, resuspension (cloud-borne aerosol particles are resuspended and become interstitial aerosol particles due to the evaporation of cloud droplets), aqueous chemistry and wet scavenging.

In the ECPP approach, the aerosol species and aerosol precursor gases are carried on the CAM grid, while cloud variables are carried on the CRM grid. Large scale transport of the aerosol and gas tracers and several “non-cloud” processes (emissions, vertical turbulent mixing, dry deposition, gas-phase chemistry, condensation/evaporation of gases on aerosols, aerosol nucleation, and aerosol coagulation) are calculated on the CAM grid. The resulting tracer distributions are passed to ECPP, in which information from the CRM is used to better simulate cloud processing of aerosols and trace species (i.e., vertical transport, aerosol activation/resuspension, aqueous chemistry, convective transport, and precipitation scavenging). The resulting aerosol fields from ECPP are then used in the CRM for cloud microphysics (droplet nucleation) and aerosol optical property calculations.

Besides using cloud statistics from the CRM instead of those from the conventional cloud parameterizations in CAM5 to drive aerosol and chemical processing by clouds, the ECPP approach differs from that in the conventional CAM5 in several other important aspects. First, the ECPP approach predicts both interstitial aerosols and cloud-borne (in-cloud) aerosols in all clouds, while the conventional CAM5 does not treat cloud-borne aerosols in convective clouds. So the conventional CAM5 needs to assume a convective-cloud activation fraction for each mode, which is used in computing in-cloud scavenging. In the ECPP approach, the cloud-borne aerosols in convective clouds are predicted through aerosol activation/resuspension associated with vertical transport, and entrainment/detrainment in convective up- and downdrafts (Sect. 2.3.3). Second, the ECPP approach treats convective transport, aqueous chemistry, and wet scavenging in an integrated, self-consistent way. The conventional CAM5 uses the

**A multi-scale aerosol climate model**

M. Wang et al.

Title Page

Abstract

Introduction

Conclusions

References

Tables

Figures



Back

Close

Full Screen / Esc

Printer-friendly Version

Interactive Discussion



process-split approach to treat convective transport, wet scavenging and aqueous chemistry in convective clouds. The grid-mean tracer concentrations are used to calculate tracer changes from each of these processes. In the real atmosphere, however, all these processes (convective transport, aqueous chemistry, and wet scavenging) occur concurrently in convective draft regions, and the resulting tracer concentrations can be significantly different from those in the ambient atmosphere. Using the grid-mean tracer concentrations in the convective draft regions may therefore bias results. In the ECPP approach, the continuity equation is integrated for convective draft regions, accounting for transport, aqueous chemistry, and wet scavenging in an integrated way (Sect. 2.3.3).

In the ECPP approach, the CRM cells on each GCM grid column are first classified into 12 different classes, according their vertical velocities, hydrometer mixing ratios, and precipitating rates (Sect. 2.3.1). Once the class of each CRM cell is determined, fractional area, mass fluxes, entrainment and detrainment rates, and micro-physical variables are diagnosed based on cloud fields from the CRM for each class (Sect. 2.3.2). These parameters are used to solve the continuity equation of tracer species for each class, which includes convective transport, activation/resuspension, aqueous chemistry, and wet scavenging (Sect. 2.3.3). The details of the ECPP approach are documented below.

### 2.3.1 Classifications of CRM cells in each GCM grid

The CRM grid cells within each GCM grid column are first categorized into updraft, downdraft and quiescent classes, based on their vertical velocities. The quiescent class contains cells with small vertical velocities. A single updraft and a single downdraft class are used in this study. Gustafson et al. (2008) also tested a multiple updraft and downdraft scheme and found no substantial improvement compared with the single updraft and downdraft scheme.

The updraft and downdraft classes are determined by comparing the vertical velocity at each CRM grid cell within a GCM grid with threshold values. The root-mean-square

## A multi-scale aerosol climate model

M. Wang et al.

[Title Page](#)

[Abstract](#)

[Introduction](#)

[Conclusions](#)

[References](#)

[Tables](#)

[Figures](#)

[⏪](#)

[⏩](#)

[◀](#)

[▶](#)

[Back](#)

[Close](#)

[Full Screen / Esc](#)

[Printer-friendly Version](#)

[Interactive Discussion](#)



upwards (positive) and downwards (negative) vertical velocities ( $w_{\text{up,rms}}$  and  $w_{\text{down,rms}}$ ) at each layer in a GCM column are calculated first. The local vertical velocity thresholds that determine updraft and downdraft classes are  $w_{\text{up,rms}}$  and  $-w_{\text{down,rms}}$ , respectively. These thresholds are only applied to the layers below the updraft/downdraft centers. (The updraft center is defined as the  $w_{\text{up,rms}}$ -weighted average of the layer index, and similarly for downdraft.) For the layers above the updraft/downdraft centers, column-wide thresholds are also used. These column-wide thresholds are calculated in a way similar to the local thresholds, based on the root-mean-square upwards and downwards vertical velocities in each column. For those layers above the updraft (or downdraft) center, the larger one of the local and column-wide updraft (or downdraft) thresholds is used. The column-wide threshold is used to in part filter out gravity wave activity at upper levels of the CRM. Following Xu et al. (1995), the updraft and downdraft classes determined by using the vertical velocity are further adjusted based on the total condensate (cloud water+cloud ice) and precipitating hydrometeor mixing ratio. Updraft and downdraft are only allowed to exist at the CRM grids that have either cloud condensate larger than  $10^{-5} \text{ kg kg}^{-1}$  or precipitating hydrometeor mixing ratio larger than  $10^{-4} \text{ kg kg}^{-1}$ . The CRM grids that do not meet these vertical velocity, condensate, and precipitation criteria are classified as the quiescent class.

Each transport class is further classified into liquid cloud and non-liquid subclasses based on a threshold liquid cloud water content of  $10^{-6} \text{ kg kg}^{-1}$ . (We subsequently use cloudy and clear when referring to the liquid-cloud and non-liquid-cloud subclasses.) Ice water is not included in the classification of the cloudy (liquid) and clear (non-liquid) subclasses since aqueous chemistry, activation, and in-cloud wet scavenging are limited to liquid clouds, as in the standard CAM5. Convective transport and aerosol activation/resuspension are calculated in each of these 6 subclasses. Each subclass is further classified into precipitating and non-precipitating (or very weakly precipitating) sub-subclasses based on a threshold precipitation rate of  $10^{-6} \text{ kg m}^{-2} \text{ s}^{-1}$ . Cloud chemistry is calculated in each of 6 cloudy (liquid) sub-subclasses, and wet scavenging is calculated in each of these 12 sub-subclasses.

**A multi-scale aerosol climate model**

M. Wang et al.

[Title Page](#)[Abstract](#)[Introduction](#)[Conclusions](#)[References](#)[Tables](#)[Figures](#)[◀](#)[▶](#)[◀](#)[▶](#)[Back](#)[Close](#)[Full Screen / Esc](#)[Printer-friendly Version](#)[Interactive Discussion](#)

### 2.3.2 Calculation of entrainment and detrainment rate

Once the class of each CRM grid cell has been determined, the horizontal area fraction ( $A_j$ ) and the vertical mass flux ( $M_j$ ) for each of 6 subclasses (cloudy and clear subclasses for each of three transport classes, and  $j$  is the subclass index) are calculated for each GCM grid cell. In computing these statistics, CRM variables are first time-averaged over the GCM time step (10 min), then grid-cell classification and class horizontal averaging are performed. The profiles of vertical mass fluxes are then used to diagnose up- and downdraft entrainment ( $E_j$ ) and detrainment ( $D_j$ ) rates, using the following mass balance equation:

$$\frac{\partial M_j}{\partial z} = E_j - D_j, \quad (1)$$

where  $z$  denotes height. In order to yield a unique expression of  $E_j$  and  $D_j$ , an assumption similar to Arakawa and Schubert (1974) is applied, such that  $D_j$  is zero if  $M_j$  increases with altitude, and  $E_j$  is zero if  $M_j$  decreases with altitude. Equation (1) does not include entrainment and detrainment associated with area changes in drafts ( $\partial A / \partial t$ ), which were treated in Gustafson et al. (2008). In the MMF implementation of ECPP, the subclass tracer concentrations are not saved from one GCM time step to the next, and effects of up/downdraft area changes between GCM time steps are not treated (see more details in Sect. 2.3.3).

These entrainment and detrainment rates are further classified by the source or destination subclass, respectively:  $E_{j,j'}$  is the entrainment into subclass  $j$  from subclass  $j'$ , and  $D_{j,j'}$  is the detrainment from subclass  $j$  to subclass  $j'$ .  $E_{j,j'}$  and  $D_{j,j'}$  are derived from  $E_j$  and  $D_j$  with the following assumptions. First, entrainment in cloudy (or clear) updraft and detrainment in clear (or cloudy) updraft are assigned to (i.e., compensated by) each other, as much as possible. The same is done for downdrafts. Any remaining unassigned detrainment for up- and downdraft subclasses is assigned to the quiescent subclasses, with preference for clear (or cloudy) draft detrainment compensating clear (or cloudy) quiescent entrainment. Any remaining unassigned entrainment for up- and

Title Page

Abstract

Introduction

Conclusions

References

Tables

Figures

◀

▶

◀

▶

Back

Close

Full Screen / Esc

Printer-friendly Version

Interactive Discussion



downdraft subclasses is assigned to the quiescent subclasses, in proportion to the clear/cloudy quiescent fractional areas. After these steps, any remaining unassigned detrainment and entrainment will only exist for the quiescent subclasses, they will be equal in magnitude, and they are assigned to each other.

### 5 2.3.3 Solving the continuity equation

The continuity equation for the mixing ratio of trace species  $l$  in the subclass  $j$  ( $q_{j,l}$ ) can then be used to solve for changes in tracer mixing ratios at each level from convective transport, aqueous chemistry, and wet scavenging:

$$\frac{\rho A_j \partial q_{j,l}}{\partial t} = - \sum_{j'} \frac{\partial (M_{j,j'} q_{j',l})}{\partial z} + \sum_{j'} E_{j,j'} q_{j',l} - D_j q_{j,l} + S_{\text{aqu\_wet},j,l}, \quad (2)$$

10 where  $S_{\text{aqu\_wet},j,l}$  is the source/sink term from aqueous chemistry and wet scavenging, and  $M_{j,j'}$  is the vertical mass flux from subclass  $j'$  to  $j$ . For quiescent subareas, vertical transport between clear-clear, clear-cloudy, and cloudy-cloudy subarea pairs is treated, and the relative amounts are determined by the quiescent clear and cloudy areas for two adjacent layers. For up- and downdraft subareas, only transport within a subclass  
 15 is treated (i.e.,  $j=j'$ ). As a result, vertical transport from clear updraft at layer  $k$  to cloudy updraft at layer  $k+1$  is treated as transport to clear updraft at layer  $k+1$ , followed by detrainment from clear to cloudy updraft at layer  $k+1$ . This is an implementation decision that is not expected to have much impact on ECPP results.

For aerosol species, activation and resuspension associated with entrainment and  
 20 detrainment must be included. Let  $li$  be an interstitial (i.e., outside cloud droplets) aerosol species (e.g., accumulation mode number or sulfate mass), and let  $la$  be the corresponding activated (i.e., cloud-borne) species. The continuity equations for the two species are:

$$\frac{\rho A_j \partial (q_{j,li})}{\partial t} = - \sum_{j'} \frac{\partial [M_{j,j'} (q_{j',li} (1 - f_{\text{act-vert},j,j',li}) + q_{j',la} f_{\text{res-vert},j,j',la})]}{\partial z}$$

Title Page

Abstract

Introduction

Conclusions

References

Tables

Figures

◀

▶

◀

▶

Back

Close

Full Screen / Esc

Printer-friendly Version

Interactive Discussion



$$\frac{\rho A_j \partial(q_{j,la})}{\partial t} = - \sum_{j'} \frac{\partial [M_{j,j'}(q_{j',li} f_{\text{act-vert},j,j',li} + q_{j',la}(1 - f_{\text{res-vert},j,j',la}))]}{\partial z}$$

$$+ \sum_{j'} E_{j,j'} [q_{j',li}(1 - f_{\text{act-ent},j,j',li}) + q_{j',la} f_{\text{res-ent},j,j',la}] - D_j q_{j,li} + S_{\text{aqu-wet},j,li}$$

$$+ \sum_{j'} E_{j,j'} [q_{j',li} f_{\text{act-ent},j,j',li} + q_{j',la}(1 - f_{\text{res-ent},j,j',la})] - D_j q_{j,la} + S_{\text{aqu-wet},j,la}$$

Here  $f_{\text{res-vert},j,j',li}$  is the fraction of the activated aerosol species that is resuspended during vertical transport from one layer to an adjacent layer, and  $f_{\text{res-ent},j,j',li}$  is the fraction resuspended when air is entrained into subclass  $j$  from  $j'$ . The  $f_{\text{res}}$  are 1 (or 0) whenever air is moving into a clear (or cloudy) subarea. The  $f_{\text{act-vert},j,j',li}$  is the fraction of the interstitial aerosol species that is activated during vertical transport from one layer to an adjacent layer, and  $f_{\text{act-ent},j,j',li}$  is the fraction activated when air is entrained into subarea  $j$  from  $j'$ . Aerosol activation occurs when 1) air moves upwards from a clear to a cloudy subarea and 2) air is entrained from a clear subarea into a cloudy subarea with upwards vertical velocity. The  $f_{\text{act}}$  are calculated based on the Abdul-Razzak and Ghan (2000) parameterization using the vertical velocity of the destination subarea.

Additional activation/resuspension associated with the turbulent vertical mixing into and out of the quiescent cloud is calculated in each GCM column, using the CAM5 routine for GCM vertical mixing with activation/resuspension (Liu et al., 2010). Activation is assumed to occur as turbulent mixing carries the air into the base of the cloud, and particles are resuspended as interstitial aerosols when turbulent mixing carries the air outside of clouds (Ovtchinnikov and Ghan, 2005). The subgrid vertical velocity ( $\sigma_w$ ) from the turbulent mixing at each GCM grid is the root-mean-square vertical velocity of the quiescent class, which includes the contribution from both the resolved and subgrid vertical velocity in the CRM grids. A lower bound of  $0.20 \text{ m s}^{-1}$  is used for the subgrid vertical velocity, the same as that used in the standard CAM5. The eddy diffusivity is diagnosed from the subgrid vertical velocity ( $\sigma_w$ ) and the mixing length (Wang

## A multi-scale aerosol climate model

M. Wang et al.

Title Page

Abstract

Introduction

Conclusions

References

Tables

Figures

◀

▶

◀

▶

Back

Close

Full Screen / Esc

Printer-friendly Version

Interactive Discussion



and Penner, 2009). The mixing length is calculated based on Holtslag and Boville (1993). This vertical mixing and the associated activation/resuspension could have been incorporated into the ECPP governing equations and code. Treating it separately is another implementation decision: advective transport and turbulent mixing are often treated in separate steps in atmospheric models; doing so here and using the CAM mixing/activation routine save effort.

Aerosol activation calculated in ECPP, which affects the aerosols, is distinct from the activation calculated in the CRM microphysics scheme (Sect. 2.2), which affects droplet number. In the CRM microphysics scheme, the vertical velocity at each CRM grid point and the GCM grid-cell mean aerosol concentrations are used for activation, while in ECPP, the subclass vertical velocities and aerosol concentrations are used. Though the treatment of activations in ECPP is somewhat inconsistent with that in the CRM, they are in fact coupled since ECPP uses updraft statistics from the CRM, and the CRM uses aerosol statics from ECPP. Some inconsistency is inevitable due to the “parameterized” aspects of the Explicit-Cloud-Parameterized-Pollutant approach.

Aqueous chemistry is calculated in each of 6 cloudy sub-subclasses (precipitating and non-precipitating sub-subclasses for each of 3 cloudy transport classes), using the CAM5 cloud-chemistry routine. Mean cloud water for the sub-subclasses is used to calculate the uptake and reaction of gas species in cloud water, which increases the mass of some cloud-borne aerosol species. A pH value of 4.5 is assumed in cloud droplet, following Liu et al. (2005). Aqueous chemistry can result in Aitken mode particles growing to a size that is nominally within the accumulation mode size range. We use the approach in Easter et al. (2004) to transfer part of the Aitken mode number and mass (those particles on the upper tail of the distribution) to the accumulation mode, the same approach as that in the standard CAM5.

In the ECPP, the wet removal of gas and aerosol species is treated by using cloud and precipitation fields in each of 12 sub-subclasses. In-cloud scavenging is applied only to the activated (i.e., cloud-borne) aerosol. The first-order loss rate for in-cloud scavenging in each sub-subclass is calculated from the loss rate of liquid cloud water

**A multi-scale aerosol climate model**

M. Wang et al.

[Title Page](#)[Abstract](#)[Introduction](#)[Conclusions](#)[References](#)[Tables](#)[Figures](#)[I◀](#)[▶I](#)[◀](#)[▶](#)[Back](#)[Close](#)[Full Screen / Esc](#)[Printer-friendly Version](#)[Interactive Discussion](#)

to precipitation in the microphysics scheme of the SAM model, and is averaged to a GCM time step of 10 min. Below cloud scavenging of aerosol is calculated as in CAM5 and Easter et al. (2004). In-cloud and below-cloud scavenging of trace gases (e.g., SO<sub>2</sub>, H<sub>2</sub>O<sub>2</sub>) are calculated assuming reversible uptake to cloud and rain drops.

5 Aqueous oxidation of SO<sub>2</sub> in rain is not yet treated.

The lifetime of updrafts and downdrafts are usually longer than the time step of the GCM model component in the MMF, which is 10 min in this study. Gustafson et al. (2008) found that using a 2 h lifetime for drafts gave best results when simulating transport of inert tracers with ECPP. Following the original Gustafson et al. (2008) approach would require 1) determining when (i.e., with GCM time step) the up- and downdrafts should begin their 2 h life cycle, 2) saving the ECPP subclass tracer concentrations from one GCM time step to the next and setting the updraft and downdraft fraction area to zero every two hours; and 3) applying grid-cell average changes calculated in the GCM (for emissions, turbulent mixing, gas phase chemistry) to the ECPP subclass mixing ratios. Instead, we adopt a modified ECPP approach that avoids these complexities while mimicing the finite lifetimes of up- and downdrafts. At the beginning of each ECPP time step, draft areas are set to zero, and quiescent areas (cloudy and clear) are determined by the previous time step liquid cloud fraction. Tracer concentrations in the quiescent subclasses are initialized to the GCM grid-cell average values at each level, with some adjustment to deal with the distribution of interstitial aerosols in cloudy (liquid) versus clear (non-liquid) subclasses. The subclass areas are then changed to their current time step values (as diagnosed from the CRM results). Aerosol activation (associated with the cloudy subclass area increases) or resuspension (associated with the cloudy subclass area decreases) are calculated. (Up/downdraft areas increase from 0, but individual quiescent areas may increase or decrease). Quiescent subclass tracer concentrations are saved at this point. Next, the tracer continuity equation (Eq. 2) is integrated for twelve 10-min steps. For each of these integrations, the quiescent subclass tracer concentrations are initialized to the earlier saved values, while the up- and downdraft tracer concentrations are carried over from the previous

## A multi-scale aerosol climate model

M. Wang et al.

[Title Page](#)

[Abstract](#)

[Introduction](#)

[Conclusions](#)

[References](#)

[Tables](#)

[Figures](#)

[◀](#)

[▶](#)

[◀](#)

[▶](#)

[Back](#)

[Close](#)

[Full Screen / Esc](#)

[Printer-friendly Version](#)

[Interactive Discussion](#)



integration. The tracer tendencies at the end of each of twelve steps are averaged together and the averaged tendencies are used to produce the final ECPP tracer concentrations. In this hybrid approach to treating time-dependent up- and downdrafts, the drafts evolve over 2 h, while the quiescent subclasses essentially evolve over 10 min, but interact with drafts with a range of ages. This new approach was tested for transport of inert tracers and gave results very close to the original method of Gustafson et al. (2008).

## 2.4 Emissions and set-up of simulations

The host GCM CAM5 uses the finite-volume dynamical core, with 30 vertical levels at  $4^\circ \times 5^\circ$  horizontal grid spacing. The GCM time step is 10 min. Climatological sea surface temperature and sea ice are used. The embedded CRM includes 32 columns at 4-km horizontal grid spacing and 28 layers coinciding with the lowest 28 CAM levels. The time step for the embedded CRM is 20 s. The model was integrated for 3 years and 2 months. Results from the last 3 years are used in this study.

Anthropogenic  $\text{SO}_2$ , black carbon, and primary organic carbon emissions are from the Lamarque et al. (2010) IPCC AR5 emission data set. (The year 2000 emissions are used in this study.) An OM/OC ratio of 1.4 is used to convert OC emissions to OM emissions. This emission data set does not provide injection heights, so injection height profiles for forest and grass fire emissions are taken from the AEROCOM unified emissions (Dentener et al., 2006), and  $\text{SO}_2$  from energy and industry sectors is emitted at 100–300 m. Volcanic  $\text{SO}_2$  and DMS emissions are also taken from Dentener et al. (2006), and 2.5% of  $\text{SO}_2$  emissions are emitted as primary sulfate aerosol. Aerosol number emissions are derived from mass emissions using species densities and volume mean emissions diameters ( $D_{\text{emit}}$ ), which vary with species and emissions sector. The  $D_{\text{emit}}$  follow recommendations in Dentener et al. (2006), with some changes that reflect values used in other studies and account for BC and OM emissions going into the model's accumulation mode. The  $D_{\text{emit}}$  values are  $0.134 \mu\text{m}$  for BC, OM, and sulfate from forest fire, grass fire, waste, and volcano (50%) sectors

## A multi-scale aerosol climate model

M. Wang et al.

Title Page

Abstract

Introduction

Conclusions

References

Tables

Figures

◀

▶

◀

▶

Back

Close

Full Screen / Esc

Printer-friendly Version

Interactive Discussion



that go into the accumulation mode; 0.261  $\mu\text{m}$  for sulfate from energy, industry, and shipping sectors that go into the accumulation mode; and 0.0504  $\mu\text{m}$  for sulfate from domestic, transportation, and volcano (50%) sectors that go into the Aitken mode. In the CAM5 simplified SOA mechanism (Liu et al., 2010), gas-phase SOA (SOA gas or SOAG) is emitted directly in the model using prescribed yields for several primary VOC classes, rather than being formed by atmospheric oxidation. The VOC emissions are taken from the MOZART-2 data set (Horowitz et al., 2003), and assumed yields are 5% (by mass) for big alkane and big alkene, 15% to toluene, 4% for isoprene, and 25% for monoterpene classes.

Emissions of sea salt and mineral dust aerosols are calculated on line. The sea salt emissions parameterization follows Martensson et al. (2003). Particles with diameters between 0.02–0.08, 0.08–1.0, and 1.0–10.0  $\mu\text{m}$  are placed in the Aitken, accumulation, and coarse modes, respectively. Mineral dust emissions are calculated with the Dust Entrainment and Deposition Model. The implementation in CAM has been described in Mahowald et al. (2006a, b) and Yoshioka et al. (2007). Particles with diameters between 0.1–1.0 and 1.0–10.0  $\mu\text{m}$  are placed in the accumulation and coarse modes, respectively.

### 3 Aerosol budgets and distributions

#### 3.1 Annual global budgets of aerosols and gas species

The global budgets of the simulated aerosols and their precursor species in the MMF model are shown in Tables 1–6, which also lists ranges of results from other model studies. For gas species, a range of results from other models, which includes the results from Liu et al. (2005) and those cited in Liu et al. (2005), are given, and for aerosol species, the average, median, and standard deviation of all available models from the model intercomparison study in Aerosol Model Intercomparison Initiative (AeroCOM) (Textor et al., 2006) are listed. More than a dozen models were included in the AeroCom intercomparison study.

## A multi-scale aerosol climate model

M. Wang et al.

Title Page

Abstract

Introduction

Conclusions

References

Tables

Figures

◀

▶

◀

▶

Back

Close

Full Screen / Esc

Printer-friendly Version

Interactive Discussion



**A multi-scale aerosol climate model**

M. Wang et al.

[Title Page](#)[Abstract](#)[Introduction](#)[Conclusions](#)[References](#)[Tables](#)[Figures](#)[⏪](#)[⏩](#)[◀](#)[▶](#)[Back](#)[Close](#)[Full Screen / Esc](#)[Printer-friendly Version](#)[Interactive Discussion](#)

The simulated DMS burden is 0.03 Tg S with a lifetime of 0.56 day, which are at the low end of other model studies (DMS burden ranges from 0.02–0.15 Tg S, and lifetime ranges from 0.5–3.0 days) (Table 1, top). The smaller DMS burden in this study is partly caused by high concentrations of NO<sub>3</sub> oxidant (not shown), especially at middle to high latitudes during local summer, in this version of the model. About 3% of DMS is located above 5 km, and 0.5% of DMS is located in the polar regions (south of 80° S and north of 80° N, which comprises 1.5% of the earth's surface area). The simulated SO<sub>2</sub> burden is 0.58 Tg S with a lifetime of 2.5 days, which are at the high end of those from other model studies (0.2–0.6 Tg S, and 0.6–2.6 days) (Table 1, middle). This is consistent with the low dry deposition rate, which removes 15.8 Tg S yr<sup>-1</sup> (compared with 16.0–55.0 Tg S yr<sup>-1</sup> in other studies). Wet scavenging removes 5.8 Tg S yr<sup>-1</sup>, 28% of which is from convective clouds. 29% of SO<sub>2</sub> is located above 5 km and 1.2% of SO<sub>2</sub> is located in the polar regions. The simulated H<sub>2</sub>SO<sub>4</sub> burden is 4.8 × 10<sup>-4</sup> Tg S with a lifetime of 15.0 min, which are greater than other studies (Table 1, bottom). The longer H<sub>2</sub>SO<sub>4</sub> lifetime can be explained by a large amount of H<sub>2</sub>SO<sub>4</sub> located above 5 km (64%) where the condensation sink is low because of low preexisting aerosol surface area. The SOA gas burden is 0.12 Tg (Table 4). The only sink of SOA gas is the condensation, which is 68.33 Tg yr<sup>-1</sup>. This gives a SOA gas lifetime of 0.64 days, although this value is somewhat misleading since the SOA gas and aerosol are in quasi-equilibrium (Liu et al., 2010).

The sulfate burden is 0.95 Tg S with a lifetime of 5.4 days, which is larger than the AeroCOM mean (0.66 Tg S and 4.12 days). The larger sulfate burden in MMF is caused by a smaller wet removal rate coefficient (the inverse of the resident time) (0.16 day<sup>-1</sup> vs. 0.22 day<sup>-1</sup>) (Table 2). The MMF model simulates a larger fraction of sulfate located above 5 km than that in AeroCOM (41% vs. 32%), with a much smaller fraction of sulfate in the polar regions than that in AeroCOM (0.73% vs. 5.91%). The larger mass fraction above 5 km and smaller mass fraction in the polar regions are also true for other aerosol species (see below). Difference in the partitioning of wet scavenging among stratiform and convective clouds and in the long range transports between the

MMF model and AeroCOM models may lead to these differences. Convective clouds (i.e., convective updraft and downdraft, see Sect. 2.3.1) account for 29% of sulfate wet scavenging in the MMF model.

The global annual burden of black carbon (BC) is 0.12 Tg, which is only half of the AeroCOM mean (0.24 Tg) (Table 3, top). This is largely explained by a smaller BC emission (7.5 Tg yr<sup>-1</sup> vs. 11.90 Tg yr<sup>-1</sup>), but also partly due to a somewhat shorter lifetime (6.0 days vs. 7.1 days in AeroCOM). The shorter lifetime, compared to AeroCOM, is partially due to neglect of BC aging in the three-mode aerosol treatment. Convective clouds account for about 32% of BC wet scavenging in the MMF model, which is slightly higher than that of sulfate aerosols and reflects the tropical biomass burning sources of BC.

The primary organic carbon (POM) burden is 0.88 Tg, which is about half of the AeroCOM mean (1.7 Tg) (Table 3, bottom). This is mainly caused by a smaller POM emission in the MMF model (48.5 Tg yr<sup>-1</sup> vs. 96.6 Tg yr<sup>-1</sup> in AeroCOM). The POM lifetime is 6.7 days, similar to those in AeroCOM models. Convective clouds contribute 32% to POM wet scavenging. The simulated SOA burden is 1.1 Tg. Many of the AeroCOM models did not explicitly simulate SOA, but included some SOA sources in their POM emissions. Our 2.0 Tg burden for POM and SOA combined is fairly close to the AeroCOM mean POM burden. The SOA lifetime is 5.8 days (Table 4), which is shorter than that of POM. This is caused by a large wet scavenging rate coefficient of SOA, which can be explained by a larger hygroscopicity parameter of SOA (Liu et al., 2010) and by the fact that SOA is produced mainly in the low latitudes (with more precipitation) from the condensation of SOA (g) emitted near surface. The mass fraction of SOA located above 5 km is 38%, which is larger than that of POM (30%).

The simulated dust burden is 33.6 Tg, which is larger than the AeroCOM median (20.50 Tg) (Table 5). This is mainly caused by the large dust emission in the MMF model. The total dust emission is 3884 Tg yr<sup>-1</sup> in CAM5, which almost doubles the median of the AeroCOM models (1840 Tg yr<sup>-1</sup>). The large dust emission in the MMF model may be caused by larger surface wind speeds or drier soil. We use the same

## GMDD

3, 1625–1695, 2010

### A multi-scale aerosol climate model

M. Wang et al.

Title Page

Abstract

Introduction

Conclusions

References

Tables

Figures

◀

▶

◀

▶

Back

Close

Full Screen / Esc

Printer-friendly Version

Interactive Discussion



dust emission parameterization as CAM5, without any tuning to the surface wind speed and soil moisture climatologies of the MMF model. The accumulation mode dust burden is 3.17 Tg and accounts for 9.4% of the total dust burden, similar to the AeroCOM median (10.80%). The mass fraction of dust located above 5 km is 13%, which is similar to the AeroCOM median. Because of the larger particle size, the mass fraction of dust above 5 km is less than that of sulfate, BC, and POM.

The simulated sea salt burden is 8.93 Tg, which is larger than the AeroCOM median (6.47 Tg) (Table 6). This is partly because sea salt in the MMF model has a longer lifetime (1.1 days) than that in the AeroCOM models (the median lifetime of 0.42 days). The fine mode sea salt mass fraction is 7.2%, which is similar to the median value of the AeroCOM models (8.72%). Convective clouds account for 34% of sea salt wet scavenging, which is somewhat higher than that of the other aerosol species, and can be attributed to removal over tropical oceans.

### 3.2 Simulated global and vertical distributions of aerosols and gas species

Figure 1 shows the vertically integrated annual mean column burdens for sulfate, BC, POM, SOA, dust and sea salt. Sulfate burden is high over the strong source regions (e.g., East Asia, and the Eastern United States), and over the Northernmost Africa. The peak over the Northernmost Africa is caused by a combination of high oxidant concentrations and reduced precipitation scavenging in that region. We noticed that a similar peak over the Northernmost Africa was also simulated in Mann et al. (2010). BC burden is high over regions with strong fossil fuel emissions (East Asia and South Asia) and biomass burning emissions (Central Africa and South America). POM demonstrates a similar spatial pattern as BC, but the maximum POM burden is located over regions with strong biomass burning emissions, while the BC burden is slightly larger over regions with strong fossil fuel emissions than over regions with strong biomass burning emissions. The maximum SOA burdens are located over Southern Africa, South and East Asia, and South America. Dust burden is larger over strong dust source regions (Northern Africa, Northwest China, and Australia), and over the downwind of

## A multi-scale aerosol climate model

M. Wang et al.

Title Page

Abstract

Introduction

Conclusions

References

Tables

Figures

◀

▶

◀

▶

Back

Close

Full Screen / Esc

Printer-friendly Version

Interactive Discussion



dust source regions (40°–60° N in the Western Pacific, and 10°–30° N in the Atlantic). Sea salt burden is high in the subtropics over both hemispheres, despite stronger sea salt emissions over the high latitudes. Less precipitation over the subtropics leads to the accumulation of sea salt. In the Southern Ocean, strong precipitation together with strong emissions leads to moderate sea salt burden.

Figure 2 shows annual averaged zonal mean mass concentrations for sulfate, BC, POM, SOA, dust and sea salt. Sulfate zonal distribution demonstrates strong anthropogenic contributions in the NH and shows a strong zonal and vertical gradient. Sulfate concentrations decrease by an order of magnitude from 30° N to the poles. BC concentrations show two peaks, one located around 30° N, due to fossil fuel emissions, and the other located in the tropics, due to biomass burning emissions. BC concentrations are much lower in the Antarctic than in the Arctic region because of much less BC emissions in the SH middle and high latitudes. POM concentrations show two similar peaks as BC. Unlike BC, however, the peak in the tropics is stronger because the emission factor of POM from biomass burning is relatively higher than that from fossil fuel. SOA concentrations have similar spatial distributions as POM. Dust concentrations show a stronger peak in the NH subtropics and a much weaker peak in the SH subtropics. The subtropic regions are located in the descending branch of Hadley circulation, where major deserts are located. Dust concentrations extend vertically into the upper troposphere. Simulated sea salt concentrations are stronger in the SH than that in the NH, because of large open ocean areas in the SH. The peak located in 50° S is caused by strong surface wind speeds and large ocean areas over that region. Two other peaks located over the subtropics are most likely caused by the less efficient wet scavenging because of less precipitation over those regions.

Figure 3 shows annual mean aerosol number concentrations in the surface layer for the Aitken, accumulation, and coarse modes. The spatial distributions of accumulation mode aerosol number concentrations are closely related to anthropogenic emissions. In the regions with strong anthropogenic emissions (e.g., East Asia, South Asia, and South America), the accumulation mode aerosol number concentrations exceed

**A multi-scale aerosol climate model**

M. Wang et al.

[Title Page](#)[Abstract](#)[Introduction](#)[Conclusions](#)[References](#)[Tables](#)[Figures](#)[◀](#)[▶](#)[◀](#)[▶](#)[Back](#)[Close](#)[Full Screen / Esc](#)[Printer-friendly Version](#)[Interactive Discussion](#)

1000 cm<sup>-3</sup>. The accumulation mode aerosol number concentrations are also high in the polluted outflow regions over oceans (e.g., 40°–60° N over the East Pacific; tropical Atlantic, and tropical East Pacific). The accumulation mode aerosol number concentrations can be as low as 40 cm<sup>-3</sup> in remote areas. Aerosol number concentrations in the Aitken mode are high over land in the regions with strong sulfur emissions in the transport and domestic sectors (e.g., the United States, Europe, and East Asia). This is not surprising since sulfur emissions in the transport and domestic sectors are the only sources of primary Aitken mode particles over land in the three-mode treatment. Aerosol number concentrations in the Aitken mode are lower over land in regions with strong biomass burning emissions. This is in part because all primary carbonaceous aerosols are emitted into the accumulation mode in the three-mode treatment, and in part because high concentrations of accumulation mode particles slow down the generation of Aitken particles from nucleation. Over oceanic regions, aerosol number concentrations in the Aitken mode are about 200–500 cm<sup>-3</sup>, which is in part from the emission of Aitken mode sea salt particles and is in part from enhanced aerosol nucleation due to low accumulation mode aerosol number concentrations. However, the Aitken mode number concentrations are lower over the oceanic regions with a large number of coarse mode particles (Fig. 4) (e.g., 0°–30° N in the Atlantic, and 50°–60° S in the Southern Ocean), which is caused by the lower aerosol nucleation due to the lower H<sub>2</sub>SO<sub>4</sub> concentrations (not shown) from the condensation of H<sub>2</sub>SO<sub>4</sub> onto the coarse mode particles. The coarse mode number concentration is highest over the source regions of dust and sea salt particles and in the downwind of dust source regions, and are generally lower than 10 cm<sup>-3</sup>.

Figure 4 shows annual zonal mean aerosol number concentrations. Simulated accumulation mode aerosol number concentrations show three peaks over the tropics, 30° N, and 50° N. The peak over the tropics results from biomass burning aerosols. The peak at 30° N is caused by pollution from South and East Asia, and the peak around 50° N is caused by pollution from Europe. The peak over tropics extends more to the upper levels compared with the other two peaks, and is caused by biomass

**A multi-scale aerosol climate model**

M. Wang et al.

[Title Page](#)[Abstract](#)[Introduction](#)[Conclusions](#)[References](#)[Tables](#)[Figures](#)[◀](#)[▶](#)[◀](#)[▶](#)[Back](#)[Close](#)[Full Screen / Esc](#)[Printer-friendly Version](#)[Interactive Discussion](#)

burning emission which is injected at 0–6 km. The Aikten mode aerosol number concentrations show a prominent peak in the tropical upper troposphere, where relative humidity is high and preexisting aerosol surface area is low, both of which favor the binary homogeneous nucleation of  $\text{H}_2\text{SO}_4$  and  $\text{H}_2\text{O}$ . Another peak occurs in the middle troposphere over the SH high latitudes, which is associated with aerosol nucleation in the austral summer (not shown). The spatial distribution of coarse mode aerosol number concentrations is similar to the spatial distributions of dust and sea salt mass concentrations (Fig. 2).

Figures 5 and 6 show the global distribution of CCN concentrations at 0.1% supersaturation in the surface, and zonal mean CCN concentrations, respectively. The spatial distribution of CCN concentrations is similar to that of the accumulation mode aerosol number concentrations. One difference between the spatial distributions of CCN concentrations and the accumulation mode aerosol number concentrations is that CCN concentrations peak in around  $20^\circ$ – $30^\circ$  N, but the accumulation mode number concentrations peak in the tropical regions. The peak in the tropical regions in the accumulation mode number concentrations is caused by carbonaceous aerosol particles due to biomass burning emission, but these carbonaceous aerosol particles are less efficient to act as CCN than sulfate aerosol particles because carbonaceous aerosols are less hygroscopic.

## 4 Comparison with observations

### 4.1 Aerosol mass concentrations

Figures 7 and 8 compare modeled DMS and  $\text{SO}_2$  vertical profiles with those from three field experiments (PEM-Tropics A, September–October, 1996; PEM-Tropics B, March–April, 1999; TRACE-P, February–April, 2001). Vertical profile data are composites of observations binned into altitude ranges (Emmons et al., 2000). Model results are monthly mean, and averaged over the observational domain. In general, simulated DMS concentrations agree well with observations, and both the model and

## A multi-scale aerosol climate model

M. Wang et al.

Title Page

Abstract

Introduction

Conclusions

References

Tables

Figures

⏪

⏩

◀

▶

Back

Close

Full Screen / Esc

Printer-friendly Version

Interactive Discussion



**A multi-scale aerosol climate model**

M. Wang et al.

[Title Page](#)[Abstract](#)[Introduction](#)[Conclusions](#)[References](#)[Tables](#)[Figures](#)[◀](#)[▶](#)[◀](#)[▶](#)[Back](#)[Close](#)[Full Screen / Esc](#)[Printer-friendly Version](#)[Interactive Discussion](#)

observations show a strong gradient from the surface to the free troposphere. The model overestimates DMS concentrations in the boundary layer over the Japan coast and over Hawaii, and underestimates DMS concentrations in the free troposphere over the China coast. Unlike DMS, observed SO<sub>2</sub> concentrations show a much weaker gradient from the surface to the free troposphere. Over some locations, there are even elevated SO<sub>2</sub> layers in the middle and upper troposphere (e.g., Christmas-Island, PEM-TROPICS A). Simulated SO<sub>2</sub> also demonstrates a much weaker gradient from the surface to the free troposphere, and elevated SO<sub>2</sub> layers are simulated over some locations. In general, simulated SO<sub>2</sub> concentrations are in reasonable agreement with observations. However, the model overestimates SO<sub>2</sub> concentrations over Christmas Island and Guam, especially in the upper troposphere. The overestimation in the upper troposphere is also evident in some other locations (e.g., Tahiti, PEM-TROPICS A). The overestimation in the middle and upper troposphere may indicate too strong vertical transport, and/or too weak in-cloud aqueous chemistry in the MMF model.

Figures 9 and 10 compare simulated annual mean surface SO<sub>2</sub> and sulfate concentrations with observations from the United States Interagency Monitoring of Protected Visual Environment (IMPROVE) sites (<http://vista.cira.colostate.edu/improve/>), the European Monitoring and Evaluation Programme (EMEP) sites (<http://www.emep.int>), and the ocean network sites operated by the University of Miami (Arimoto et al., 1996; Prospero et al., 1989; Savoie et al., 1989, 1993). Simulated SO<sub>2</sub> concentrations are in reasonable agreement with observations at a large number of European sites, while simulated SO<sub>2</sub> concentrations are overestimated at the IMPROVE sites in the United States. Sulfate concentrations are in reasonable agreement with observations. The agreement is particularly good in Europe (within a factor two) (Fig. 9). Over the United States, sulfate concentrations at most sites agree with observations within a factor of 2, but the model overestimates sulfate concentrations for some sites, which are mostly located in the Western United States (Fig. 9). Over the oceanic sites operated by the University of Miami, sulfate concentrations in the MMF model are in reasonable agreement with observations.

**A multi-scale aerosol climate model**

M. Wang et al.

[Title Page](#)[Abstract](#)[Introduction](#)[Conclusions](#)[References](#)[Tables](#)[Figures](#)[◀](#)[▶](#)[◀](#)[▶](#)[Back](#)[Close](#)[Full Screen / Esc](#)[Printer-friendly Version](#)[Interactive Discussion](#)

Modeled surface BC and OC concentrations are compared with those observed at the IMPROVE sites, EMEP sites, and those compiled by Liousse et al. (1996), Cooke et al. (1999), and Zhang et al. (2007) in Figs. 11 and 12. In general, the model underestimated BC concentrations, by a factor of 2–4, especially at the EMEP sites. In the three-mode representation of aerosols in CAM5, BC particles are assumed to be internally mixed with sulfate and other aerosols particles in the accumulation mode, which may overestimate the wet removal rate of BC particles, although the BC lifetime is only slightly smaller than the AeroCOM mean (Table 3). Simulated OC concentrations agree better with observations. At the IMPROVE sites, the model agrees with observations within a factor of two, while the model underestimates OC concentrations at the EMEP sites, and overestimates OC concentrations in some sites compiled by Liousse et al. (1996) and Cooke et al. (1999).

Sea salt and dust concentrations are compared with those observed at the ocean network sites operated by the University of Miami in Figs. 13 and 14, respectively. Both dust and sea salt are in reasonable agreement with observations. However, dust concentrations are underestimated at high latitude sites (two sites over Antarctic, and one site over Ireland), which may suggest that the wet scavenging rate of dust particles are too strong or the polarward transport is too weak. The underestimation of dust in the high latitudes is consistent with the low mass fraction in the polar regions compared with that in the AeroCOM models (Table 5).

Simulated BC vertical profiles are compared with those measured in several recent aircraft campaigns at tropical and middle latitudes (Fig. 15) and at high latitudes (Fig. 16) by using Single Particle Soot absorption Photometers (SP2s) (Schwarz et al., 2006). The SP2 instrument uses laser-induced incandescence to detect and size individual BC particles, which enables SP2 to detect and characterize individual BC particles in real-time, and make it suitable for continuous particle measurements from the surface to the lower stratosphere on board aircraft. Monthly mean model results are averaged at several locations along the flight tracks (see map symbols in Figs. 15 and 16).

**A multi-scale aerosol climate model**

M. Wang et al.

[Title Page](#)[Abstract](#)[Introduction](#)[Conclusions](#)[References](#)[Tables](#)[Figures](#)[⏪](#)[⏩](#)[◀](#)[▶](#)[Back](#)[Close](#)[Full Screen / Esc](#)[Printer-friendly Version](#)[Interactive Discussion](#)

Measured BC concentrations show a strong gradient from the surface to the middle altitudes in the tropics (CR-AVE, and TC4) and subtropics (AVE Houston), with BC concentrations around  $100 \text{ ng kg}^{-1}$  in the surface and  $1 \text{ ng kg}^{-1}$  at 500 hPa. The modeled BC concentrations also show a strong gradient from the surface to the middle troposphere. However, the gradient is much weaker in the MMF model, which leads to the overestimations in the middle and upper troposphere, a common problem in most AeroCOM models (Fig. 9 in Koch et al., 2009). In the middle latitudes, observed BC vertical profiles show a smaller gradient between the surface and the middle troposphere than in the tropics. The model does a better job in simulating BC vertical profiles in the middle latitude than in the tropics, but BC concentrations are overestimated in the upper troposphere, and underestimated in the surface.

The observed BC vertical profiles in the high latitudes peak in the middle troposphere in April, a feature that is not observed in June–July. The MMF model underestimates BC concentrations in the lower and middle troposphere and overestimates BC concentrations above 200 hPa in April. The model simulates BC vertical profiles better in the summer. The underestimation at the higher latitudes (Fig. 16) and the overestimation at the lower latitudes (Fig. 15) are common problems in almost all the AeroCOM models (Table 8 in Koch et al., 2009). As suggested by Koch et al. (2009), this may point to a problem in distinguishing between removal of BC by convective and stratiform clouds. The MMF model has a more physically-based treatment for wet scavenging from convective clouds (Sect. 2.3); however this improvement still did not solve the problem, though the MMF model did simulate aerosols in the high latitudes better than the standard CAM5 (Wang et al., 2010).

## 4.2 Aerosol number and size distributions

Figure 17 shows aerosol size distributions in the marine boundary layer. The observational data is from Heintzenberg et al. (2000), and were compiled and aggregated onto a  $15^\circ \times 15^\circ$  grid. The model data is sampled over the same regions as those of the observations. The observational data clearly shows a bimodal distribution in the marine

boundary layer, with an Aitken mode with a geometric mean diameter of 20–50 nm and an accumulation mode with a geometric mean diameter of 100–200 nm. The MMF model reproduces the observed bimodal distribution in most regions. Simulated Aitken mode aerosol number concentrations are generally in good agreement with observations in most latitude bands. The improved simulation of the Aitken mode aerosol number concentrations compared with some previous studies (Pierce and Adams, 2006; Wang et al., 2009) may come from the inclusion of both sea salt particles in the Aitken mode and the boundary layer nucleation mechanism in the model. However, the model underestimates the accumulation mode aerosol number concentrations, especially over the low and middle latitude bands. This may suggest that the model underestimates fine mode sea salt, polluted outflow from continents or the growth of Aitken mode particles. Wang et al. (2009) showed that the underestimation of fine mode sea salt particles in their model was consistent with their underestimation of accumulation mode aerosol number concentrations.

Figure 18 compares simulated aerosol size distributions in the free troposphere with observations. Unlike the marine boundary layer, observations in the free troposphere show a monomodal distribution at all sites except for the Lindenberg 4 km observations. For that case, the large accumulation mode number concentration came from one flight where the accumulation mode number concentration was  $250 \text{ cm}^{-3}$ , while the remaining 4 flights gave an average accumulation mode number concentration of  $15 \text{ cm}^{-3}$  (Petzold et al., 2002). The observed monomodal size distribution in the free troposphere is believed to result from the depletion of accumulation mode particles in the boundary layer, and the generation of Aitken particles from nucleation in the free troposphere (Raes et al., 2000). The model does simulate a prominent Aitken mode at all sites, and the Aitken mode number concentrations are generally larger over the low latitudes than over the high latitudes, and at high altitudes than at low altitudes, which indicates the influence of aerosol nucleation. Simulated accumulation mode number concentrations are lower than that of the Aitken mode. The accumulation mode concentrations are overestimated in the middle and upper troposphere, especially over

**A multi-scale aerosol climate model**

M. Wang et al.

[Title Page](#)[Abstract](#)[Introduction](#)[Conclusions](#)[References](#)[Tables](#)[Figures](#)[◀](#)[▶](#)[◀](#)[▶](#)[Back](#)[Close](#)[Full Screen / Esc](#)[Printer-friendly Version](#)[Interactive Discussion](#)

Southern Florida (CRYSTAL-FACE). However, it should be noted that the observations from CRYSTAL-FACE only represent a single date. Simulated Aitken mode diameters are generally underestimated. The difficulties in simulating the monomodal size distributions in the free troposphere may partly come from the modal representation of aerosol size distribution in the MMF model. We noticed that Wang et al. (2009), who also used a modal approach, had difficulties in simulating the monomodal size distributions in the free troposphere too. Fixed standard deviations and fixed modal boundaries used in the most modal aerosol approaches may limit their capability to simulate monomodal aerosol size distribution in the free troposphere.

Figure 19 shows vertical profiles of the aerosol number concentrations in the Aitken mode (diameter > 14 nm), and in the accumulation mode (diameter > 100 nm) from both the model and observations at Punta Arena, Chile and Prestwick, Scotland (Minikin et al., 2003). The observed Aitken mode aerosol number concentrations are around  $1000\text{ cm}^{-3}$  over Scotland, and are around  $500\text{ cm}^{-3}$  over Southern Chile. The model simulates the Aitken mode number concentration in the low troposphere over Southern Chile reasonably well, and performs better than some previous studies (Wang et al., 2009). This may come from the inclusion of ultrafine sea salt emissions, and the boundary layer nucleation mechanism in the MMF. However, the model slightly underestimates the Aitken mode number concentration over Scotland in the lower free troposphere, which may be partly explained by the fact that carbonaceous aerosols are emitted into the accumulation mode in the three-mode treatment. The model overestimates the Aitken mode particle number concentrations in the upper troposphere and stratosphere. This may suggest that nucleation in the upper troposphere is overestimated, consistent with the overestimation of  $\text{SO}_2$  concentration in the upper troposphere (Fig. 8).

Observed accumulation mode aerosol number concentrations decrease with altitude in the lower troposphere, are nearly constant with altitude in the middle troposphere, and increases slightly with altitude in the upper troposphere. The model reproduces the decreasing accumulation mode number concentrations with altitude in the lower

**A multi-scale aerosol climate model**

M. Wang et al.

[Title Page](#)[Abstract](#)[Introduction](#)[Conclusions](#)[References](#)[Tables](#)[Figures](#)[I◀](#)[▶I](#)[◀](#)[▶](#)[Back](#)[Close](#)[Full Screen / Esc](#)[Printer-friendly Version](#)[Interactive Discussion](#)

**A multi-scale aerosol climate model**

M. Wang et al.

[Title Page](#)[Abstract](#)[Introduction](#)[Conclusions](#)[References](#)[Tables](#)[Figures](#)[⏪](#)[⏩](#)[◀](#)[▶](#)[Back](#)[Close](#)[Full Screen / Esc](#)[Printer-friendly Version](#)[Interactive Discussion](#)

free troposphere, with a slight overestimation over Southern Chile, and underestimation over Scotland. The model also simulates an increasing accumulation number concentration with altitude in the middle and upper troposphere. However, the increases with altitude are stronger in the model than that in the observations, and the model overestimates the accumulation mode number concentration in the upper troposphere.

Figure 20 compares simulated vertical profiles of CCN concentrations at 0.1% supersaturation with results from eight field experiments. (See Ghan et al., 2001 for the details of each experiment.) The model simulates decreasing CCN concentrations with increasing altitude over all eight locations, while the observations demonstrate a variety of vertical profiles. The elevated CCN concentrations over Tasmania during SOCEX-1 and ACE-1 may come from the continental outflow from Australia, and the monthly mean model results may not catch the continental outflow. The elevated CCN concentrations over the Arctic may come from poleward pollution transport in the free troposphere, and is consistent with the observed BC profiles (Fig. 14). The model did not catch this feature, although it did simulate elevated BC concentrations to some extent (Fig. 14). The observed CCN concentrations show strong seasonal variations over Tasmania, with higher concentrations in the austral summer (SOCEX-2), and much lower concentrations in the austral winter (SOCEX-1). The model also produces this seasonal variation, but the seasonal contrast in the model is much weaker than that in the observations. In general, simulated CCN vertical profiles are within the observed variations, except over the ARM site in Oklahoma. The ARM site is located in a concentration gradient region. Given the coarse resolution used in the MMF model, the model may not be able to accurately simulate the strong gradient in CCN concentrations. The model performance is qualitatively similar to the results of Ghan et al. (2001).

### 4.3 Aerosol optical properties

Figure 21 compares modeled monthly aerosol optical depth (AOD) and single scattering albedo (SSA) with observational data from the AERONET (<http://aeronet.gsfc.nasa.gov/>) at sites in East and South Asia, Europe, Northern and Southern Africa, North and

South America. Simulated AOD agrees with observations within a factor of 2 for most AERONET sites. The model simulates AOD well in North America. However, it underestimates AOD in East Asia, South Asia, and Europe, and it overestimates AOD in Northern Africa. The overestimation in Northern Africa is consistent with the MMF's large dust burden compared with the AeroCOM models (Table 5). Simulated SSA is also in reasonable agreement with observations, and ranges from 0.78 to 0.98. SSA is higher in North America than in Northern Africa and East Asia, which is caused by less absorbing aerosols (carbonaceous aerosols and/or dust aerosols) in North America. The model simulates a smaller variation in SSA than that in observations for all regions except in South Africa. For example, SSA in North America ranges from 0.89–0.96 in the model, but it ranges from 0.76 to 0.99 in the observations.

Figure 22 compares modeled annual-averaged aerosol optical depth at 550 nm with that from a satellite AOD retrieval composite derived by Kinne et al. (2006). The satellite composite combines the strength of individual satellite retrievals (MODIS, MISR, AVHRR, TOMS, and POLDER), giving regional preferences separately over land and over ocean. Among all satellite retrievals, those with the minimum difference to the regional AERONET average are selected to contribute to the satellite composite. The model simulates reasonable spatial patterns, with large AOD over regions with strong fossil fuel and biomass burning emissions and over the source regions of dust aerosols, and with low AOD over remote regions. However, the model overestimates AOD over the dust source regions (Northern Africa, and the middle Asia), and it underestimates AOD over the regions with strong fossil fuel and biomass burning emissions, which is consistent with the comparison with the AERONET observations (Fig. 21). The model also underestimates AOD over the Southern Ocean, which may be caused by the underestimation of sea salt aerosols.

**A multi-scale aerosol climate model**

M. Wang et al.

[Title Page](#)[Abstract](#)[Introduction](#)[Conclusions](#)[References](#)[Tables](#)[Figures](#)[I◀](#)[▶I](#)[◀](#)[▶](#)[Back](#)[Close](#)[Full Screen / Esc](#)[Printer-friendly Version](#)[Interactive Discussion](#)

## 5 Summary

In this study, a new multiscale aerosol climate model was developed that has several major extensions to the Colorado State University multi-scale modeling framework (MMF) model, and consists of three components. The global climate model (GCM) component is the NCAR CAM5 and includes a modal aerosol treatment that uses three log-normal modes to represent aerosol size distributions. The cloud resolving model (CRM) component is SAM, which has a two-moment microphysics scheme that predicts mass and number mixing ratios for several hydrometer categories. The CRM is embedded in each GCM grid column to replace the GCM's conventional parameterizations of moist convection and large scale condensation and to permit the explicit simulation of convective clouds. The third component of this multiscale aerosol climate model is the Explicit-Cloud-Parameterized-Pollutant (ECP) approach, which uses cloud statics diagnosed from the CRM component of the MMF model to drive the aerosol and gas processing by clouds (convective transport, activation/resuspension, wet scavenging, and aqueous chemistry). The ECP approach allows explicit simulation of the effects of convective clouds on aerosols while keeping the computational cost acceptable. Simulated aerosol fields from the GCM component and the ECP approach are used at each CRM grid for aerosol activation. The aerosol water uptake is also calculated at each CRM grid cell, which accounts for the subgrid variation in relative humidity on each GCM grid. With these updates, this multi-scale aerosol climate model includes the treatment of aerosol and chemical processes, and allows us to study aerosol effects on climate from cumulus to global scales.

Simulated global, annual aerosol budgets from this multi-scale aerosol climate model are within the range of results from the other models included in the AeroCOM intercomparison (Textor et al., 2006). However, the mass fractions of aerosols located above 5 km are larger than those of the AeroCOM models, except dust, which is similar to that of the AeroCOM models. In contrast, the MMF model produces a much smaller mass fraction of aerosols in the polar regions. Differences in poleward transport or in

## A multi-scale aerosol climate model

M. Wang et al.

[Title Page](#)

[Abstract](#)

[Introduction](#)

[Conclusions](#)

[References](#)

[Tables](#)

[Figures](#)

[◀](#)

[▶](#)

[◀](#)

[▶](#)

[Back](#)

[Close](#)

[Full Screen / Esc](#)

[Printer-friendly Version](#)

[Interactive Discussion](#)



the treatment of wet removal processes may contribute to the differences between the MMF model and the AeroCOM models. Convective clouds contribute to around 30% of the total aerosol wet removal.

5 Simulated DMS vertical profiles agree well with observations, while the model overestimates SO<sub>2</sub> concentrations in the upper troposphere in some locations. Simulated surface sulfate, dust and sea salt concentrations are in reasonable agreement with observations. OC concentrations are in reasonable agreement with observations in the United States, but are underestimated in Europe. The model underestimates surface BC concentrations, which may partly arise from the fact that BC is assumed internally  
10 mixed with other aerosols in the accumulation mode. The model overestimates BC concentrations in the upper troposphere over the tropics and underestimates BC concentrations in the Arctic regions, a common problem in other global aerosol models (Koch et al., 2009).

The model simulates a bimodal aerosol size distribution in the marine boundary  
15 layer, which is consistent with observations. However, the MMF model underestimates accumulation mode number concentrations, which may suggest that the model underestimates fine mode sea salt, pollution outflow from continents or the growth of Aitken mode particles. Simulated aerosol size distributions in the free troposphere show a prominent Aitken mode, but they also show a weak accumulation mode that is  
20 not present in the observational data. Simulated Aitken mode aerosol number concentrations in the upper troposphere over the middle latitudes are overestimated, which is consistent with the excessive SO<sub>2</sub> concentrations in the upper troposphere. Simulated accumulation mode number concentrations are overestimated in the middle and upper troposphere. The overestimation of accumulation mode number concentrations in the  
25 middle and upper troposphere is consistent with the large aerosol mass fraction above 5 km in the MMF model compared with the AeroCOM models. The simulated CCN concentrations are within the observed variations.

Simulated AOD and SSA are in reasonable agreement with observations at AERONET sites. The MMF model also simulates reasonable spatial patterns of AOD

## A multi-scale aerosol climate model

M. Wang et al.

[Title Page](#)

[Abstract](#)

[Introduction](#)

[Conclusions](#)

[References](#)

[Tables](#)

[Figures](#)

[I◀](#)

[▶I](#)

[◀](#)

[▶](#)

[Back](#)

[Close](#)

[Full Screen / Esc](#)

[Printer-friendly Version](#)

[Interactive Discussion](#)



compared with the satellite composite, although the model overestimates AOD over dust source regions, and it underestimates AOD over the source regions of strong fossil fuel and biomass burning emissions.

One limitation of this study is the lack of high-order turbulence schemes in the CRM, which biases the lower level clouds in the MMF model (Wang et al., 2010). Since low clouds are important components of the global climate system, the bias in low clouds may bias simulated aerosols, and further aerosol effects on climate. This will be addressed in a future study, in which we will include a high-order turbulence scheme (Golaz et al., 2002; Larson and Golaz, 2005) in the CRM component of the MMF model and explore how it will affect simulated low clouds and aerosols.

Overall, the PNNL-MMF multi-scale aerosol climate model simulates aerosols and aerosol optical properties as well as other aerosol models. In a separate paper (Wang et al., 2010), we will use this model to study aerosol indirect effects, and to examine the relationship between aerosol fields and cloud fields.

*Acknowledgements.* This work was supported by the NASA Interdisciplinary Science Program under grant NNX07AI56G. We thank Phil Rasch for helpful discussion regarding the treatment of convective transport of tracer species in GCMs. We are also grateful to Stefan Kinne for providing the satellite AOD retrieval composite data used in Fig. 22.

## References

- Abdul-Razzak, H. and Ghan, S. J.: A parameterization of aerosol activation 2. Multiple aerosol types, *J. Geophys. Res.*, 105, 6837–6844, 2000.
- Andreae, M. O., Rosenfeld, D., Artaxo, P., Costa, A. A., Frank, G. P., Longo, K. M., and Silva-Dias, M. A. F.: Smoking rain clouds over the Amazon, *Science*, 303, 1337–1342, 2004.
- Arakawa, A. and Schubert, W. H.: Interaction of a cumulus cloud ensemble with large-scale environment 1., *J. Atmos. Sci.*, 31, 674–701, 1974.
- Arimoto, R., Duce, R. A., Savoie, D. L., Prospero, J. M., Talbot, R., Cullen, J. D., Tomza, U., Lewis, N. F., and Jay, B. J.: Relationships among aerosol constituents from Asia and the North Pacific during PEM-West A, *J. Geophys. Res.*, 101, 2011–2023, 1996.

## A multi-scale aerosol climate model

M. Wang et al.

[Title Page](#)

[Abstract](#)

[Introduction](#)

[Conclusions](#)

[References](#)

[Tables](#)

[Figures](#)

[⏪](#)

[⏩](#)

[◀](#)

[▶](#)

[Back](#)

[Close](#)

[Full Screen / Esc](#)

[Printer-friendly Version](#)

[Interactive Discussion](#)



## A multi-scale aerosol climate model

M. Wang et al.

[Title Page](#)

[Abstract](#)

[Introduction](#)

[Conclusions](#)

[References](#)

[Tables](#)

[Figures](#)

[◀](#)

[▶](#)

[◀](#)

[▶](#)

[Back](#)

[Close](#)

[Full Screen / Esc](#)

[Printer-friendly Version](#)

[Interactive Discussion](#)



Bechtold, P., Redelsperger, J. L., Beau, I., Blackburn, M., Brinkop, S., Grandpeix, J. Y., Grant, A., Gregory, D., Guichard, F., Hoff, C., and Ioannidou, E.: A GCSS model inter-comparison for a tropical squall line observed during TOGA-COARE. II: Intercomparison of single-column models and a cloud-resolving model, *Q. J. Roy. Meteor. Soc.*, 126, 865–888, 2000.

Chatfield, R. B. and Crutzen, P. J.: Sulfur-dioxide in remote oceanic air – cloud transport of reactive precursors, *J. Geophys. Res.*, 89, 7111–7132, 1984.

Collins, W. D., Rasch, P. J., Boville, B. A., Hack, J. J., McCaa, J. R., Williamson, D. L., Briegleb, B. P., Bitz, C. M., Lin, S. J., and Zhang, M. H.: The formulation and atmospheric simulation of the Community Atmosphere Model version 3 (CAM3), *J. Climate*, 19, 2144–2161, 2006.

Cooke, W. F., Lioussé, C., Cachier, H., and Feichter, J.: Construction of a  $1^\circ \times 1^\circ$  fossil fuel emission data set for carbonaceous aerosol and implementation and radiative impact in the ECHAM4 model, *J. Geophys. Res.*, 104, 22137–22162, 1999.

Cui, Z. Q., Carslaw, K. S., Yin, Y., and Davies, S.: A numerical study of aerosol effects on the dynamics and microphysics of a deep convective cloud in a continental environment, *J. Geophys. Res.*, 111, D05201, doi:10.1029/2005jd005981, 2006.

Del Genio, A. D., Kovari, W., Yao, M. S., and Jonas, J.: Cumulus microphysics and climate sensitivity, *J. Climate*, 18, 2376–2387, 2005.

Dentener, F., Kinne, S., Bond, T., Boucher, O., Cofala, J., Generoso, S., Ginoux, P., Gong, S., Hoelzemann, J. J., Ito, A., Marelli, L., Penner, J. E., Putaud, J.-P., Textor, C., Schulz, M., van der Werf, G. R., and Wilson, J.: Emissions of primary aerosol and precursor gases in the years 2000 and 1750 prescribed data-sets for AeroCom, *Atmos. Chem. Phys.*, 6, 4321–4344, doi:10.5194/acp-6-4321-2006, 2006.

Easter, R. C., Ghan, S. J., Zhang, Y., Saylor, R. D., Chapman, E. G., Laulainen, N. S., Abdul-Razzak, H., Leung, L. R., Bian, X. D., and Zaveri, R. A.: MIRAGE: model description and evaluation of aerosols and trace gases, *J. Geophys. Res.*, 109, D20210, doi:10.1029/2004jd004571, 2004.

Ekman, A. M. L., Wang, C., Strom, J., and Krejci, R.: Explicit simulation of aerosol physics in a cloud-resolving model: aerosol transport and processing in the free troposphere, *J. Atmos. Sci.*, 63, 682–696, 2006.

Emanuel, K. A. and Zivkovic-Rothman, M.: Development and evaluation of a convection scheme for use in climate models, *J. Atmos. Sci.*, 56, 1766–1782, 1999.

**A multi-scale aerosol climate model**

M. Wang et al.

[Title Page](#)[Abstract](#)[Introduction](#)[Conclusions](#)[References](#)[Tables](#)[Figures](#)[◀](#)[▶](#)[◀](#)[▶](#)[Back](#)[Close](#)[Full Screen / Esc](#)[Printer-friendly Version](#)[Interactive Discussion](#)

- Emmons, L. K., Hauglustaine, D. A., Muller, J. F., Carroll, M. A., Brasseur, G. P., Brunner, D., Staehelin, J., Thouret, V., and Marenco, A.: Data composites of airborne observations of tropospheric ozone and its precursors, *J. Geophys. Res.*, 105, 20497–20538, 2000.
- Ghan, S., Easter, R., Hudson, J., and Breon, F. M.: Evaluation of aerosol indirect radiative forcing in MIRAGE, *J. Geophys. Res.*, 106, 5317–5334, 2001.
- Golaz, J. C., Larson, V. E., and Cotton, W. R.: A PDF-based model for boundary layer clouds. Part I: Method and model description, *J. Atmos. Sci.*, 59, 3540–3551, 2002.
- Grabowski, W. W.: Coupling cloud processes with the large-scale dynamics using the Cloud-Resolving Convection Parameterization (CRCP), *J. Atmos. Sci.*, 58, 978–997, 2001.
- Gregory, D. and Guichard, F.: Aspects of the parametrization of organized convection: contrasting cloud-resolving model and single-column model realizations, *Q. J. Roy. Meteor. Soc.*, 128, 625–646, 2002.
- Gustafson, W. I., Berg, L. K., Easter, R. C., and Ghan, S. J.: The Explicit-Cloud Parameterized-Pollutant hybrid approach for aerosol-cloud interactions in multiscale modeling framework models: tracer transport results, *Environ. Res. Lett.*, 3, 025005, doi:10.1088/1748-9326/3/2/025005, 2008.
- Heintzenberg, J., Covert, D. C., and Van Dingenen, R.: Size distribution and chemical composition of marine aerosols: a compilation and review, *Tellus B*, 52, 1104–1122, 2000.
- Holtstlag, A. A. M. and Boville, B. A.: Local versus nonlocal boundary-layer diffusion in a global climate model, *J. Climate*, 6, 1825–1842, 1993.
- Horowitz, L. W., Walters, S., Mauzerall, D. L., Emmons, L. K., Rasch, P. J., Granier, C., Tie, X. X., Lamarque, J. F., Schultz, M. G., Tyndall, G. S., Orlando, J. J., and Brasseur, G. P.: A global simulation of tropospheric ozone and related tracers: description and evaluation of MOZART, version 2, *J. Geophys. Res.*, 108, 4784, doi:10.1029/2002jd002853, 2003.
- Iacono, M. J., Delamere, J. S., Mlawer, E. J., and Clough, S. A.: Evaluation of upper tropospheric water vapor in the NCAR Community Climate Model (CCM3) using modeled and observed HIRS radiances, *J. Geophys. Res.*, 108, 4037, doi:10.1029/2002jd002539, 2003.
- Iacono, M. J., Delamere, J. S., Mlawer, E. J., Shephard, M. W., Clough, S. A., and Collins, W. D.: Radiative forcing by long-lived greenhouse gases: calculations with the AER radiative transfer models, *J. Geophys. Res.*, 113, D13103, doi:10.1029/2008jd009944, 2008.
- IPCC: Climate Change 2007: The Physical Science Basis. Contribution of Working Group I to the Fourth Assessment Report of the Intergovernmental Panel on Climate Change, edited by: Solomon, S., Qin, D., Manning, M., Chen, Z., Marquis, M., Averyt, K. B., Tignor, M., and

## A multi-scale aerosol climate model

M. Wang et al.

[Title Page](#)

[Abstract](#)

[Introduction](#)

[Conclusions](#)

[References](#)

[Tables](#)

[Figures](#)

[◀](#)

[▶](#)

[◀](#)

[▶](#)

[Back](#)

[Close](#)

[Full Screen / Esc](#)

[Printer-friendly Version](#)

[Interactive Discussion](#)



- Miller, H. L., Cambridge University Press, Cambridge, UK and New York, NY, USA, 996 pp., 2007.
- Iversen, T. and Seland, O.: A scheme for process-tagged SO<sub>4</sub> and BC aerosols in NCAR CCM3: validation and sensitivity to cloud processes, *J. Geophys. Res.*, 107, 4751, doi:10.1029/2001jd000885, 2002.
- Jacob, D. J., Prather, M. J., Rasch, P. J., Shia, R. L., Balkanski, Y. J., Beagley, S. R., Bergmann, D. J., Blackshear, W. T., Brown, M., Chiba, M., Chipperfield, M. P., deGrandpre, J., Dignon, J. E., Feichter, J., Genthon, C., Grose, W. L., Kasibhatla, P. S., Kohler, I., Kritz, M. A., Law, K., Penner, J. E., Ramonet, M., Reeves, C. E., Rotman, D. A., Stockwell, D. Z., VanVelthoven, P. F. J., Verver, G., Wild, O., Yang, H., and Zimmermann, P.: Evaluation and intercomparison of global atmospheric transport models using Rn-222 and other short-lived tracers, *J. Geophys. Res.*, 102, 5953–5970, 1997.
- Khairoutdinov, M., Randall, D., and DeMott, C.: Simulations of the atmospheric general circulation using a cloud-resolving model as a superparameterization of physical processes, *J. Atmos. Sci.*, 62, 2136–2154, 2005.
- Khairoutdinov, M., DeMott, C., and Randall, D.: Evaluation of the simulated interannual and sub-seasonal variability in an AMIP-Style simulation using the CSU multiscale modeling framework, *J. Climate*, 21, 413–431, doi:10.1175/2007jcli1630.1, 2008.
- Khairoutdinov, M. F. and Randall, D. A.: A cloud resolving model as a cloud parameterization in the NCAR community climate system model: preliminary results, *Geophys. Res. Lett.*, 28, 3617–3620, 2001.
- Khairoutdinov, M. F. and Randall, D. A.: Cloud resolving modeling of the ARM summer 1997 IOP: model formulation, results, uncertainties, and sensitivities, *J. Atmos. Sci.*, 60, 607–625, 2003.
- Kinne, S., Schulz, M., Textor, C., Guibert, S., Balkanski, Y., Bauer, S. E., Bernsten, T., Berglen, T. F., Boucher, O., Chin, M., Collins, W., Dentener, F., Diehl, T., Easter, R., Feichter, J., Fillmore, D., Ghan, S., Ginoux, P., Gong, S., Grini, A., Hendricks, J., Herzog, M., Horowitz, L., Isaksen, I., Iversen, T., Kirkevåg, A., Kloster, S., Koch, D., Kristjansson, J. E., Krol, M., Lauer, A., Lamarque, J. F., Lesins, G., Liu, X., Lohmann, U., Montanaro, V., Myhre, G., Penner, J., Pitari, G., Reddy, S., Seland, O., Stier, P., Takemura, T., and Tie, X.: An AeroCom initial assessment – optical properties in aerosol component modules of global models, *Atmos. Chem. Phys.*, 6, 1815–1834, doi:10.5194/acp-6-1815-2006, 2006.
- Koch, D., Schulz, M., Kinne, S., McNaughton, C., Spackman, J. R., Balkanski, Y., Bauer, S.,

**A multi-scale aerosol climate model**

M. Wang et al.

[Title Page](#)[Abstract](#)[Introduction](#)[Conclusions](#)[References](#)[Tables](#)[Figures](#)[◀](#)[▶](#)[◀](#)[▶](#)[Back](#)[Close](#)[Full Screen / Esc](#)[Printer-friendly Version](#)[Interactive Discussion](#)

Berntsen, T., Bond, T. C., Boucher, O., Chin, M., Clarke, A., De Luca, N., Dentener, F., Diehl, T., Dubovik, O., Easter, R., Fahey, D. W., Feichter, J., Fillmore, D., Freitag, S., Ghan, S., Ginoux, P., Gong, S., Horowitz, L., Iversen, T., Kirkevåg, A., Klimont, Z., Kondo, Y., Krol, M., Liu, X., Miller, R., Montanaro, V., Moteki, N., Myhre, G., Penner, J. E., Perlwitz, J., Pitari, G., Reddy, S., Sahu, L., Sakamoto, H., Schuster, G., Schwarz, J. P., Seland, Ø., Stier, P., Takegawa, N., Takemura, T., Textor, C., van Aardenne, J. A., and Zhao, Y.: Evaluation of black carbon estimations in global aerosol models, *Atmos. Chem. Phys.*, 9, 9001–9026, doi:10.5194/acp-9-9001-2009, 2009.

Koren, I., Kaufman, Y. J., Remer, L. A., and Martins, J. V.: Measurement of the effect of Amazon smoke on inhibition of cloud formation, *Science*, 303, 1342–1345, 2004.

Koren, I., Kaufman, Y. J., Rosenfeld, D., Remer, L. A., and Rudich, Y.: Aerosol invigoration and restructuring of Atlantic convective clouds, *Geophys. Res. Lett.*, 32, L14828, doi:10.1029/2005gl023187, 2005.

Larson, V. E. and Golaz, J. C.: Using probability density functions to derive consistent closure relationships among higher-order moments, *Mon. Weather Rev.*, 133, 1023–1042, 2005.

Liousse, C., Penner, J. E., Chuang, C., Walton, J. J., Eddleman, H., and Cachier, H.: A global three-dimensional model study of carbonaceous aerosols, *J. Geophys. Res.*, 101, 19411–19432, 1996.

Liu, X. H., Easter, R. C., Ghan, S. J., Zaveri, R., Rasch, P., et al.: Toward a minimal representation of aerosol direct and indirect effects, *J. Climate*, in preparation, 2010.

Liu, X. H., Penner, J. E., and Herzog, M.: Global modeling of aerosol dynamics: model description, evaluation, and interactions between sulfate and nonsulfate aerosols, *J. Geophys. Res.*, 110, D18206, doi:10.1029/2004JD005674, 2005.

Lohmann, U.: Global anthropogenic aerosol effects on convective clouds in ECHAM5-HAM, *Atmos. Chem. Phys.*, 8, 2115–2131, doi:10.5194/acp-8-2115-2008, 2008.

Mahowald, N. M., Rasch, P. J., and Prinn, R. G.: Cumulus parameterizations in chemical transport models, *J. Geophys. Res.*, 100, 26173–26189, 1995.

Mahowald, N. M., Muhs, D. R., Levis, S., Rasch, P. J., Yoshioka, M., Zender, C. S., and Luo, C.: Change in atmospheric mineral aerosols in response to climate: last glacial period, preindustrial, modern, and doubled carbon dioxide climates, *J. Geophys. Res.*, 111, D10202, doi:10.1029/2005jd006653, 2006a.

Mahowald, N. M., Yoshioka, M., Collins, W. D., Conley, A. J., Fillmore, D. W., and Coleman, D. B.: Climate response and radiative forcing from mineral aerosols during the last

## A multi-scale aerosol climate model

M. Wang et al.

Title Page

Abstract

Introduction

Conclusions

References

Tables

Figures

◀

▶

◀

▶

Back

Close

Full Screen / Esc

Printer-friendly Version

Interactive Discussion



- glacial maximum, pre-industrial, current and doubled-carbon dioxide climates, *Geophys. Res. Lett.*, 33, L20705, doi:10.1029/2006gl026126, 2006b.
- Mann, G. W., Carslaw, K. S., Spracklen, D. V., Ridley, D. A., Manktelow, P. T., Chipperfield, M. P., Pickering, S. J., and Johnson, C. E.: Description and evaluation of GLOMAP-mode: a modal global aerosol microphysics model for the UKCA composition-climate model, *Geosci. Model Dev. Discuss.*, 3, 651–734, doi:10.5194/gmdd-3-651-2010, 2010.
- Martensson, E. M., Nilsson, E. D., de Leeuw, G., Cohen, L. H., and Hansson, H. C.: Laboratory simulations and parameterization of the primary marine aerosol production, *J. Geophys. Res.*, 108, 4297, doi:10.1029/2002jd002263, 2003.
- Menon, S. and Rotstajn, L.: The radiative influence of aerosol effects on liquid-phase cumulus and stratiform clouds based on sensitivity studies with two climate models, *Clim. Dyn.*, 27, 345–356, doi:10.1007/S00382-006-0139-3, 2006.
- Minikin, A., Petzold, A., Strom, J., Krejci, R., Seifert, M., van Velthoven, P., Schlager, H., and Schumann, U.: Aircraft observations of the upper tropospheric fine particle aerosol in the Northern and Southern Hemispheres at midlatitudes, *Geophys. Res. Lett.*, 30, 1503, doi:10.1029/2002gl016458, 2003.
- Mlawer, E. J., Taubman, S. J., Brown, P. D., Iacono, M. J., and Clough, S. A.: Radiative transfer for inhomogeneous atmospheres: RRTM, a validated correlated-k model for the longwave, *J. Geophys. Res.*, 102, 16663–16682, 1997.
- Morrison, H., Curry, J. A., and Khvorostyanov, V. I.: A new double-moment microphysics parameterization for application in cloud and climate models. Part I: Description, *J. Atmos. Sci.*, 62, 1665–1677, 2005.
- Morrison, H., Thompson, G., and Tatarskii, V.: Impact of cloud microphysics on the development of trailing stratiform precipitation in a simulated squall line: comparison of one- and two-moment schemes, *Mon. Weather Rev.*, 137, 991–1007, doi:10.1175/2008mwr2556.1, 2009.
- Nober, F. J., Graf, H. F., and Rosenfeld, D.: Sensitivity of the global circulation to the suppression of precipitation by anthropogenic aerosols, *Global Planet. Change*, 37, 57–80, doi:0.1016/S0921-8181(02)00191-1, 2003.
- Ovtchinnikov, M. and Ghan, S. J.: Parallel simulations of aerosol influence on clouds using cloud-resolving and single-column models, *J. Geophys. Res.*, 110, D15S10, doi:10.1029/2004jd005088, 2005.
- Ovtchinnikov, M., Ackerman, T., Marchand, R., and Khairoutdinov, M.: Evaluation of the multi-scale modeling framework using data from the atmospheric radiation measurement program,

**A multi-scale aerosol climate model**

M. Wang et al.

[Title Page](#)[Abstract](#)[Introduction](#)[Conclusions](#)[References](#)[Tables](#)[Figures](#)[◀](#)[▶](#)[◀](#)[▶](#)[Back](#)[Close](#)[Full Screen / Esc](#)[Printer-friendly Version](#)[Interactive Discussion](#)

J. Climate, 19, 1716–1729, 2006.

Petzold, A., Fiebig, M., Flentje, H., Keil, A., Leiterer, U., Schroder, F., Stifter, A., Wendisch, M., and Wendling, P.: Vertical variability of aerosol properties observed at a continental site during the Lindenberg Aerosol Characterization Experiment (LACE 98), *J. Geophys. Res.*, 107, 8128, doi:10.1029/2001jd001043, 2002.

Pierce, J. R. and Adams, P. J.: Global evaluation of CCN formation by direct emission of sea salt and growth of ultrafine sea salt, *J. Geophys. Res.*, 111, D06203, doi:10.1029/2005JD006186, 2006.

Pritchard, M. S. and Somerville, R. C. J.: Accessing the diurnal cycle of precipitation in a multi-scale climate model, *J. Adv. Model. Earth Syst.*, 1, 16, doi:10.3894/JAMES.2009.1.12, 2009a.

Pritchard, M. S. and Somerville, R. C. J.: Empirical orthogonal function analysis of the diurnal cycle of precipitation in a multi-scale climate model, *Geophys. Res. Lett.*, 36, L05812, doi:10.1029/2008GL036964, 2009b.

Prospero, J. M., Uematsu, M., and Savoie, D. L.: Mineral aerosol transport to the Pacific Ocean, in: *Chemical Oceanography*, edited by: Ridley, J. P., Chester, R., and Duce, R. A., Elsevier, New York, 188–218, 1989.

Raes, F., Van Dingenen, R., Vignati, E., Wilson, J., Putaud, J. P., Seinfeld, J. H., and Adams, P.: Formation and cycling of aerosols in the global troposphere, *Atmos. Environ.*, 34, 4215–4240, 2000.

Rasch, P. J., Feichter, J., Law, K., Mahowald, N., Penner, J., Benkovitz, C., Genthon, C., Giannakopoulos, C., Kasibhatla, P., Koch, D., Levy, H., Maki, T., Prather, M., Roberts, D. L., Roelofs, G. J., Stevenson, D., Stockwell, Z., Taguchi, S., Kritz, M., Chipperfield, M., Baldochi, D., McMurry, P., Barrie, L., Balkansi, Y., Chatfield, R., Kjellstrom, E., Lawrence, M., Lee, H. N., Lelieveld, J., Noone, K. J., Seinfeld, J., Stenchikov, G., Schwartz, S., Walcek, C., and Williamson, D.: A comparison of scavenging and deposition processes in global models: results from the WCRP Cambridge Workshop of 1995, *Tellus B*, 52, 1025–1056, 2000.

Rosenfeld, D., Lohmann, U., Raga, G. B., O'Dowd, C. D., Kulmala, M., Fuzzi, S., Reissell, A., and Andreae, M. O.: Flood or drought: how do aerosols affect precipitation?, *Science*, 321, 1309–1313, doi:10.1126/Science.1160606, 2008.

Savoie, D. I., Prospero, J. M., Larsen, R. J., Huang, F., Izaguirre, M. A., Huang, T., Snowdon, T. H., Custals, L., and Sanderson, C. G.: Nitrogen and sulfur species in Antarctic aerosols at Mawson, Palmer Station, and Marsh (King George Island), *J. Atmos. Chem.*,

17, 95–122, 1993.

Savoie, D. L., Prospero, J. M., and Saltzman, E. S.: Nitrate, nonseasalt sulfate and methanesulfonate over the Pacific Ocean, in: *Chemical Oceanography*, edited by: Ridley, J. P., Chester, R., and Duce, R. A., Elsevier, New York, 219–250, 1989.

5 Schwarz, J. P., Gao, R. S., Fahey, D. W., Thomson, D. S., Watts, L. A., Wilson, J. C., Reeves, J. M., Darbeheshti, M., Baumgardner, D. G., Kok, G. L., Chung, S. H., Schulz, M., Hendricks, J., Lauer, A., Karcher, B., Slowik, J. G., Rosenlof, K. H., Thompson, T. L., Langford, A. O., Loewenstein, M., and Aikin, K. C.: Single-particle measurements of midlatitude black carbon and light-scattering aerosols from the boundary layer to the lower stratosphere, *J. Geophys. Res.*, 111, D16207, doi:10.1029/2006jd007076, 2006.

10 Suzuki, K., Nakajima, T., Satoh, M., Tomita, H., Takemura, T., Nakajima, T. Y., and Stephens, G. L.: Global cloud-system-resolving simulation of aerosol effect on warm clouds, *Geophys. Res. Lett.*, 35, L19817, doi:10.1029/2008gl035449, 2008.

15 Tao, W. K., Chern, J. D., Atlas, R., Randall, D., Khairoutdinov, M., Li, J. L., Waliser, D. E., Hou, A., Lin, X., Peters-Lidard, C., Lau, W., Jiang, J., and Simpson, J.: A multiscale modeling system developments, applications, and critical issues, *B. Am. Meteor. Soc.*, 90, 515, doi:10.1175/2008bams2542.1, 2009.

20 Textor, C., Schulz, M., Guibert, S., Kinne, S., Balkanski, Y., Bauer, S., Berntsen, T., Berglen, T., Boucher, O., Chin, M., Dentener, F., Diehl, T., Easter, R., Feichter, H., Fillmore, D., Ghan, S., Ginoux, P., Gong, S., Grini, A., Hendricks, J., Horowitz, L., Huang, P., Isaksen, I., Iversen, I., Kloster, S., Koch, D., Kirkevåg, A., Kristjansson, J. E., Krol, M., Lauer, A., Lamarque, J. F., Liu, X., Montanaro, V., Myhre, G., Penner, J., Pitari, G., Reddy, S., Seland, Ø., Stier, P., Takemura, T., and Tie, X.: Analysis and quantification of the diversities of aerosol life cycles within AeroCom, *Atmos. Chem. Phys.*, 6, 1777–1813, doi:10.5194/acp-6-1777-2006, 2006.

25 Wang, C. and Prinn, R. G.: On the roles of deep convective clouds in tropospheric chemistry, *J. Geophys. Res.*, 105, 22269–22297, 2000.

Wang, C.: A modeling study of the response of tropical deep convection to the increase of cloud condensation nuclei concentration: 1. Dynamics and microphysics, *J. Geophys. Res.*, 110, D21211, doi:10.1029/2004jd005720, 2005.

30 Wang, M. and Penner, J. E.: Aerosol indirect forcing in a global model with particle nucleation, *Atmos. Chem. Phys.*, 9, 239–260, doi:10.5194/acp-9-239-2009, 2009.

Wang, M., Ghan, S., Ovchinnikov, M., Easter, R., Liu, X. H., et al.: Aerosol indirect effects in a multi-scale aerosol-climate model, *Atmos. Chem. Phys.*, in preparation, 2010.

**GMDD**

3, 1625–1695, 2010

---

## A multi-scale aerosol climate model

M. Wang et al.

---

Title Page

Abstract

Introduction

Conclusions

References

Tables

Figures

◀

▶

◀

▶

Back

Close

Full Screen / Esc

Printer-friendly Version

Interactive Discussion



## A multi-scale aerosol climate model

M. Wang et al.

[Title Page](#)

[Abstract](#)

[Introduction](#)

[Conclusions](#)

[References](#)

[Tables](#)

[Figures](#)

[◀](#)

[▶](#)

[◀](#)

[▶](#)

[Back](#)

[Close](#)

[Full Screen / Esc](#)

[Printer-friendly Version](#)

[Interactive Discussion](#)



Wang, M. H., Penner, J. E., and Liu, X. H.: Coupled IMPACT aerosol and NCAR CAM3 model: evaluation of predicted aerosol number and size distribution, *J. Geophys. Res.*, 114, D06302, doi:10.1029/2008jd010459, 2009.

Xie, S. C., Xu, K. M., Cederwall, R. T., Bechtold, P., Del Genio, A. D., Klein, S. A., Cripe, D. G., Ghan, S. J., Gregory, D., Iacobellis, S. F., Krueger, S. K., Lohmann, U., Petch, J. C., Randall, D. A., Rotstayn, L. D., Somerville, R. C. J., Sud, Y. C., Von Salzen, K., Walker, G. K., Wolf, A., Yio, J. J., Zhang, G. J., and Zhang, M. G.: Intercomparison and evaluation of cumulus parametrizations under summertime midlatitude continental conditions, *Q. J. Roy. Meteor. Soc.*, 128, 1095–1135, 2002.

Xu, K. M., Cederwall, R. T., Donner, L. J., Grabowski, W. W., Guichard, F., Johnson, D. E., Khairoutdinov, M., Krueger, S. K., Petch, J. C., Randall, D. A., Seman, C. J., Tao, W. K., Wang, D. H., Xie, S. C., Yio, J. J., and Zhang, M. H.: An intercomparison of cloud-resolving models with the atmospheric radiation measurement summer 1997 intensive observation period data, *Q. J. Roy. Meteor. Soc.*, 128, 593–624, 2002.

Yoshioka, M., Mahowald, N. M., Conley, A. J., Collins, W. D., Fillmore, D. W., Zender, C. S., and Coleman, D. B.: Impact of desert dust radiative forcing on Sahel precipitation: relative importance of dust compared to sea surface temperature variations, vegetation changes, and greenhouse gas warming, *J. Climate*, 20, 1445–1467, doi:10.1175/Jcli4056.1, 2007.

Zhang, J. H., Lohmann, U., and Stier, P.: A microphysical parameterization for convective clouds in the ECHAM5 climate model: single-column model results evaluated at the Oklahoma Atmospheric Radiation Measurement Program site, *J. Geophys. Res.*, 110, D15S07, doi:10.1029/2004jd005128, 2005.

Zhang, Q., Jimenez, J. L., Canagaratna, M. R., Allan, J. D., Coe, H., Ulbrich, I., Alfarra, M. R., Takami, A., Middlebrook, A. M., Sun, Y. L., Dzepina, K., Dunlea, E., Docherty, K., DeCarlo, P. F., Salcedo, D., Onasch, T., Jayne, J. T., Miyoshi, T., Shimon, A., Hatakeyama, S., Takegawa, N., Kondo, Y., Schneider, J., Drewnick, F., Borrmann, S., Weimer, S., Demerjian, K., Williams, P., Bower, K., Bahreini, R., Cottrell, L., Griffin, R. J., Rautiainen, J., Sun, J. Y., Zhang, Y. M., and Worsnop, D. R.: Ubiquity and dominance of oxygenated species in organic aerosols in anthropogenically-influenced Northern Hemisphere midlatitudes, *Geophys. Res. Lett.*, 34, L13801, doi:10.1029/2007gl029979, 2007.

**Table 1.** Global budget for DMS, SO<sub>2</sub>, and H<sub>2</sub>SO<sub>4</sub>. Values in the parenthesis show the range from other model studies, which include Liu et al. (2005) and those listed in Liu et al. (2005).

DMS	
Sources (Tg S/yr)	18.17 (10.7–23.7)
Emission (Tg S/yr)	18.17
Sinks (Tg S/yr)	18.17
Gas-phase oxidation (Tg S/yr)	18.17
Burden (Tg S)	0.03 (0.02–0.15)
Above 5 km (%)	3.07
In Polar <sup>a</sup> (%)	0.54
Lifetime (days)	0.56 (0.5–3.0)
SO <sub>2</sub>	
Sources (Tg S/yr)	84.56
Emission (Tg S/yr)	68.55 (61.2–92.0)
DMS oxidation (Tg S/yr)	16.01 (10.0–24.7)
Sinks (Tg S/yr)	84.56
Dry deposition (Tg S/yr)	15.81 (16.0–55.0)
Wet deposition (Tg S/yr)	5.81 (0–19.9)
Gas-phase oxidation (Tg S/yr)	16.58 (6.1–22.0)
Aqueous-phase oxidation (Tg S/yr)	46.36 (24.5–57.8)
Burden (Tg S)	0.58 (0.20–0.69)
Above 5 km (%)	29.37
In Polar (%)	1.16
Lifetime (days)	2.46(0.2–2.6)
Wet+dry removal rate (/day)	0.10
Wet/(wet+dry) (%)	26.86
From convective cloud <sup>b</sup> (%)	28.33
H <sub>2</sub> SO <sub>4</sub>	
Sources (Tg S/yr)	16.58
Gas-phase production (Tg S/yr)	16.58 (6.1–22.0)
Sinks (Tg S/yr)	16.58
Dry deposition (Tg S/yr)	0.01
Wet deposition (Tg S/yr)	0.06
Nucleation (Tg S/yr)	0.18
Condensation (Tg S/yr)	16.22
Aqueous-phase deposition (Tg S/yr)	0.12
Burden (Tg S)	0.00048 (9.0×10 <sup>-6</sup> –1.0×10 <sup>-3</sup> )
Above 5 km (%)	64.08
In Polar (%)	0.46
Lifetime (min)	15.2 (4.3–10.1)

<sup>a</sup> South of 80° S and north of 80° N.

<sup>b</sup> The percentage contribution of convective clouds to the total wet scavenging.

Title Page

Abstract

Introduction

Conclusions

References

Tables

Figures

◀

▶

◀

▶

Back

Close

Full Screen / Esc

Printer-friendly Version

Interactive Discussion



**Table 2.** Global budget for sulfate. The values in the parenthesis are the mean value (left) and normalized standard deviation (right, as percentage) from available models in AeroCOM (see Textor et al., 2006, Table 10). The standard deviation is normalized by the all models average in the percentage in AeroCOM.

Sources (Tg S/yr)	64.69 (59.67, 22)
Emission (Tg S/yr)	1.76
Gas-phase SO <sub>2</sub> oxidation (Tg S/yr)	16.27
Aqueous-phase SO <sub>2</sub> oxidation (Tg S/yr)	46.48
From H <sub>2</sub> O <sub>2</sub> chemistry (%)	71.61
From convective clouds (%)	23.19
Burden (Tg S)	0.95 (0.66, 25)
Aitken mode sulfate (%)	6.66
Accumulation mode sulfate (%)	91.94
Coarse mode sulfate (%)	1.41
Above 5 km (%)	40.97 (32.33, 36)
In Polar (%)	0.73 (5.91, 55)
Lifetime (days)	5.36 (4.12, 18)
Removal rate (/day)	0.19 (0.25, 18)
Wet (/day)	0.16 (0.22, 22)
Dry (/day)	0.03 (0.03, 55)
Wet/(wet+dry) (%)	86.03 (88.50, 8)
From convective clouds (%)	29

## A multi-scale aerosol climate model

M. Wang et al.

[Title Page](#)

[Abstract](#)

[Introduction](#)

[Conclusions](#)

[References](#)

[Tables](#)

[Figures](#)

[I◀](#)

[▶I](#)

[◀](#)

[▶](#)

[Back](#)

[Close](#)

[Full Screen / Esc](#)

[Printer-friendly Version](#)

[Interactive Discussion](#)



**Table 3.** Global budget for BC and POM. The values in the parenthesis are the mean value (left) and standard deviation (right) from available models in AeroCOM (see Textor et al., 2006, Table 10). The standard deviation is normalized by the all models average in the percentage in AeroCOM.

BC	
Sources (Tg/yr)	7.5(11.9, 23)
Burden (Tg)	0.12 (0.24, 42)
Above 5 km (%)	29.09(21.20, 52)
In Polar (%)	0.43(4.18, 71)
Lifetime (days)	6.02(7.12, 33)
Removal rate (/day)	0.17(0.15, 21)
Wet (/day)	0.13(0.12, 31)
Dry (/day)	0.04(0.03, 55)
Wet (%)	78.27(78.6, 18)
From convective clouds (%)	31.75
POM	
Sources (Tg/yr)	48.48 (96.60, 26)
Burden (Tg)	0.88(1.70, 27)
Above 5 km (%)	29.53(20.40, 56)
In Polar (%)	0.43(3.27, 76)
Lifetime (days)	6.73(6.54, 27)
Removal rate (/day)	0.15(0.16, 24)
Wet (/day)	0.12(0.14, 32)
Dry (/day)	0.03(0.03, 49)
Wet/(wet+dry) (%)	78.87(79.90, 16)
From convective clouds (%)	32.51

# GMDD

3, 1625–1695, 2010

## A multi-scale aerosol climate model

M. Wang et al.

Title Page

Abstract

Introduction

Conclusions

References

Tables

Figures

◀

▶

◀

▶

Back

Close

Full Screen / Esc

Printer-friendly Version

Interactive Discussion



**A multi-scale aerosol climate model**

M. Wang et al.

[Title Page](#)[Abstract](#)[Introduction](#)[Conclusions](#)[References](#)[Tables](#)[Figures](#)[I◀](#)[▶I](#)[◀](#)[▶](#)[Back](#)[Close](#)[Full Screen / Esc](#)[Printer-friendly Version](#)[Interactive Discussion](#)**Table 4.** Global budget for SOAG (gas-phase SOA) and SOA.

SOAG	
Emission (Tg/yr)	68.33
Burden (Tg)	0.12
Above 5 km (%)	0.61
In Polar (%)	0
Lifetime (days)	0.64
SOA	
Sources (Tg/yr)	68.33
Gas-phase production (Tg/yr)	68.33
Burden (Tg)	1.1
Above 5 km (%)	38.15
In Polar (%)	0.37
Lifetime (days)	5.84
Removal rate (/day)	0.17
Wet (/day)	0.15
Wet/(wet+dry) (%)	87.09
From convective clouds (%)	31.74

**A multi-scale aerosol  
climate model**

M. Wang et al.

[Title Page](#)[Abstract](#)[Introduction](#)[Conclusions](#)[References](#)[Tables](#)[Figures](#)[I◀](#)[▶I](#)[◀](#)[▶](#)[Back](#)[Close](#)[Full Screen / Esc](#)[Printer-friendly Version](#)[Interactive Discussion](#)

**Table 5.** Global budget for dust. The values in the parenthesis are the mean (left), median value (middle), and standard deviation (right) from available models in AeroCOM (see Textor et al., 2006, Table 10). The standard deviation is normalized by the all models average in the percentage in AeroCOM.

Dust	Accumulation	Coarse	Total
Sources (Tg/yr)	124.3	3760.2	3884.5 (1840, 1640, 49)
Burden (Tg)	3.17	30.37	33.55 (19.20, 20.50, 40)
Above 5 km (%)	23.95	11.87	13.02 (14.10, 14.10, 51)
In Polar (%)	0.24	0.08	0.1 (1.54, 1.00, 102)
Fine mass (%)	–	–	9.4 (20.8, 10.8, 114)
Lifetime (days)	9.5	2.96	3.17 (4.14, 4.04, 43)
Removal rate (/day)	0.11	0.34	0.32 (0.31, 0.25, 62)
Wet (/day)	0.08	0.08	0.08 (0.08, 0.09, 42)
Wet/(wet+dry) (%)	74.56	24.43	26.01 (33, 31.7, 54)
From convective clouds (%)	29.64	28.85	28.92

## A multi-scale aerosol climate model

M. Wang et al.

[Title Page](#)

[Abstract](#)

[Introduction](#)

[Conclusions](#)

[References](#)

[Tables](#)

[Figures](#)

[I◀](#)

[▶I](#)

[◀](#)

[▶](#)

[Back](#)

[Close](#)

[Full Screen / Esc](#)

[Printer-friendly Version](#)

[Interactive Discussion](#)



**Table 6.** Global budget for sea salt. The values in the parenthesis are the mean (left), median value (middle), and standard deviation (right) from available models in AeroCOM (see Textor et al., 2006, Table 10). The standard deviation is normalized by the all models average in the percentage in AeroCOM.

Sea Salt	Aikten	Accumulation	Coarse	Total
Sources (Tg/yr)	0.54	108.16	2943.23	3051.93 (16600, 6280, 199)
Burden (Tg)	0	0.64	8.29	8.93 (7.52, 6.37, 54)
Above 5 km (%)	25.75	19.91	10.54	11.22 (8.65, 6.93, 92)
In Polar (%)	2.4	0.66	0.5	0.51 (3.32, 1.88, 140)
Fine mass (%)	–	–	–	7.1 (14.60, 8.72, 118)
Lifetime (days)	2.64	2.19	1.03	1.07 (0.48, 0.41, 58)
Removal rate (/day)	0.38	0.46	0.97	0.93 (5.07, 2.50, 188)
Wet (/day)	0.18	0.38	0.47	0.46 (0.79, 0.68, 77)
Wet/(wet+dry) (%)	46.65	82.54	48.39	49.6 (30.50, 30.30, 65)
From convective clouds (%)	28.73	34.5	34.05	34.08

## A multi-scale aerosol climate model

M. Wang et al.

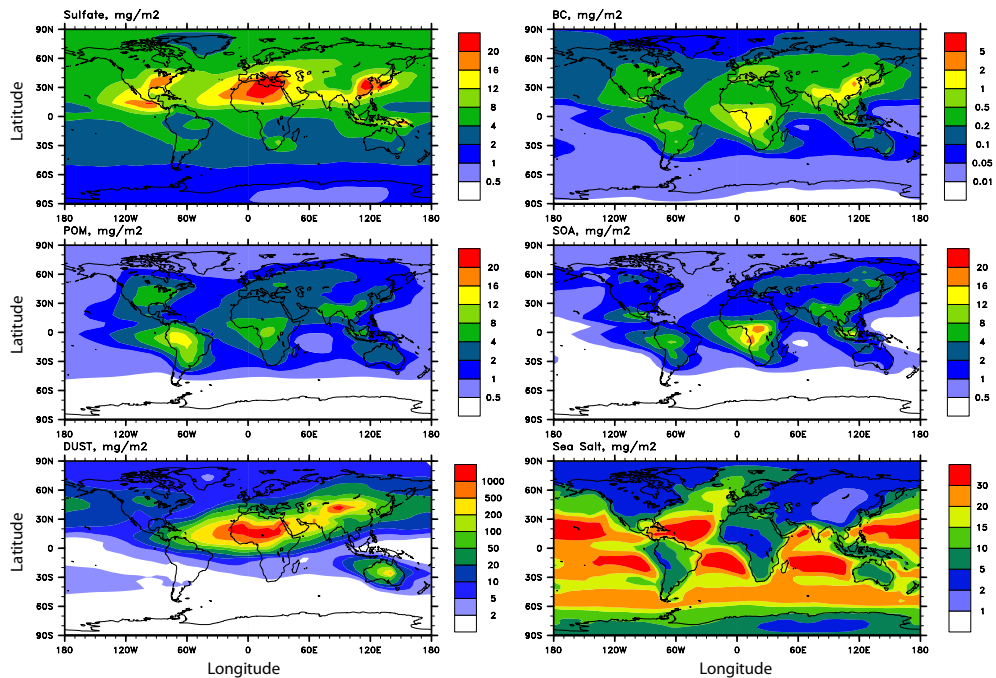


**Fig. 1.** Vertically integrated annual mean concentrations ( $\text{mg m}^{-2}$ ) of sulfate, BC, POM, SOA, dust, and sea salt predicted by the model.

[Title Page](#)[Abstract](#)[Introduction](#)[Conclusions](#)[References](#)[Tables](#)[Figures](#)[◀](#)[▶](#)[◀](#)[▶](#)[Back](#)[Close](#)[Full Screen / Esc](#)[Printer-friendly Version](#)[Interactive Discussion](#)

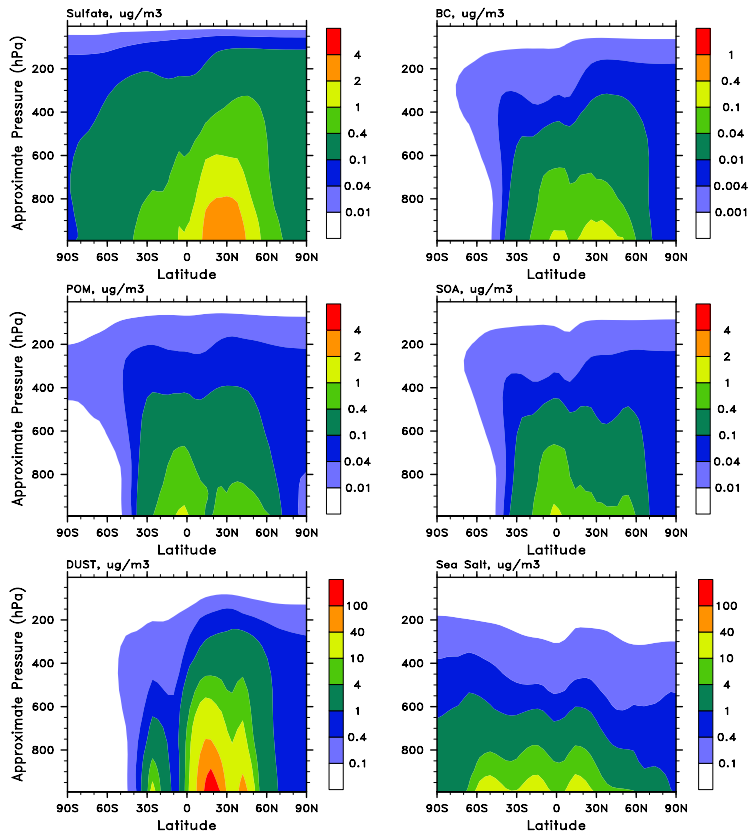


**Fig. 2.** Annual averaged zonal mean concentrations ( $\mu\text{g m}^{-3}$ ) of sulfate, BC, POM, SOA, dust and sea salt predicted by the model. The host GCM model (CAM5) used a hybrid vertical coordinate and the pressure at the  $k$ th model level is given by  $p(k)=A(k)p_0+B(k)p_s$ , where  $p_s$  is surface pressure,  $p_0$  is a specified constant pressure (1000 hPa), and  $A$  and  $B$  are coefficients. Data are plotted as a function of this hybrid vertical coordinate times 1000, and labelled “Approximate Pressure”.

**A multi-scale aerosol climate model**

M. Wang et al.

Title Page	
Abstract	Introduction
Conclusions	References
Tables	Figures
◀	▶
◀	▶
Back	Close
Full Screen / Esc	
Printer-friendly Version	
Interactive Discussion	



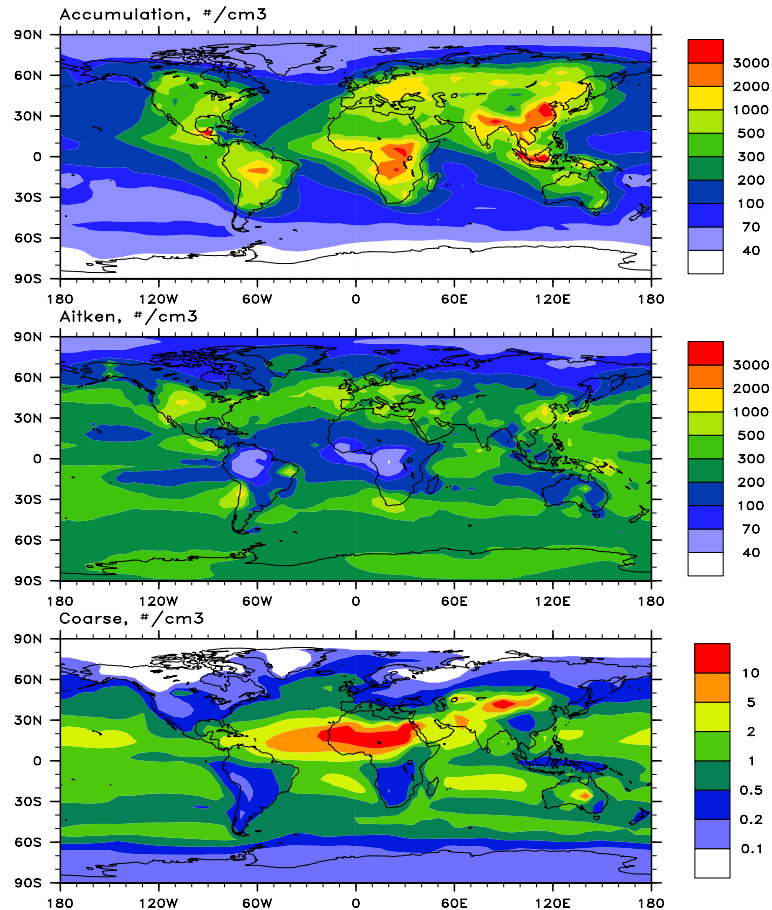


**Fig. 3.** Annual averaged global distributions of aerosol number concentrations (number  $\text{cm}^{-3}$ ) in the lowest model layer for the Aktien mode, accumulation mode, and coarse mode aerosols predicted by the model.

Title Page

Abstract

Introduction

Conclusions

References

Tables

Figures

◀

▶

◀

▶

Back

Close

Full Screen / Esc

Printer-friendly Version

Interactive Discussion



**A multi-scale aerosol climate model**

M. Wang et al.

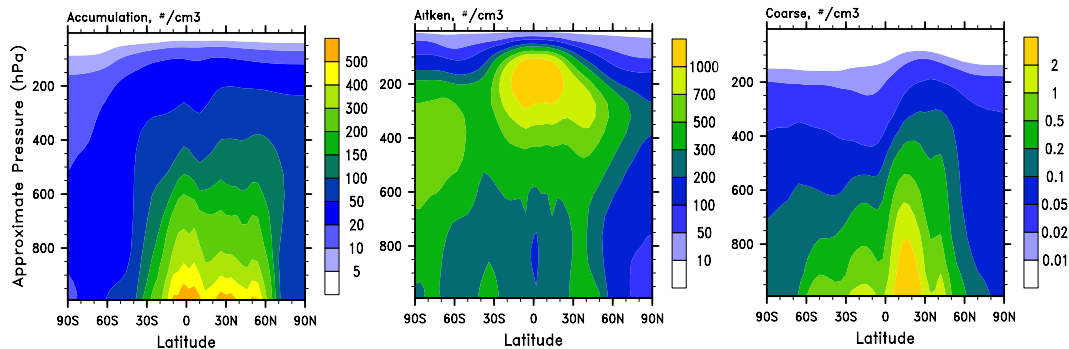


**Fig. 4.** Zonal mean aerosol number concentrations (number  $\text{cm}^{-3}$ ) for the Aitken mode, accumulation mode, and coarse mode predicted by the model.

[Title Page](#)[Abstract](#)[Introduction](#)[Conclusions](#)[References](#)[Tables](#)[Figures](#)[⏪](#)[⏩](#)[◀](#)[▶](#)[Back](#)[Close](#)[Full Screen / Esc](#)[Printer-friendly Version](#)[Interactive Discussion](#)



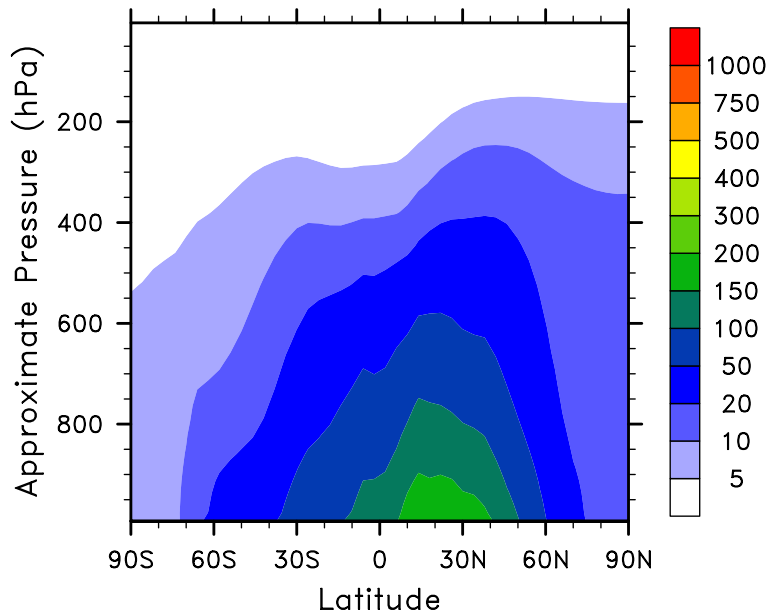


**Fig. 6.** Zonal mean CCN concentrations (number  $\text{cm}^{-3}$ ) at 0.1% supersaturation.

**A multi-scale aerosol climate model**

M. Wang et al.

[Title Page](#)

[Abstract](#)   [Introduction](#)

[Conclusions](#)   [References](#)

[Tables](#)   [Figures](#)

[⏪](#)   [⏩](#)

[◀](#)   [▶](#)

[Back](#)   [Close](#)

[Full Screen / Esc](#)

[Printer-friendly Version](#)

[Interactive Discussion](#)



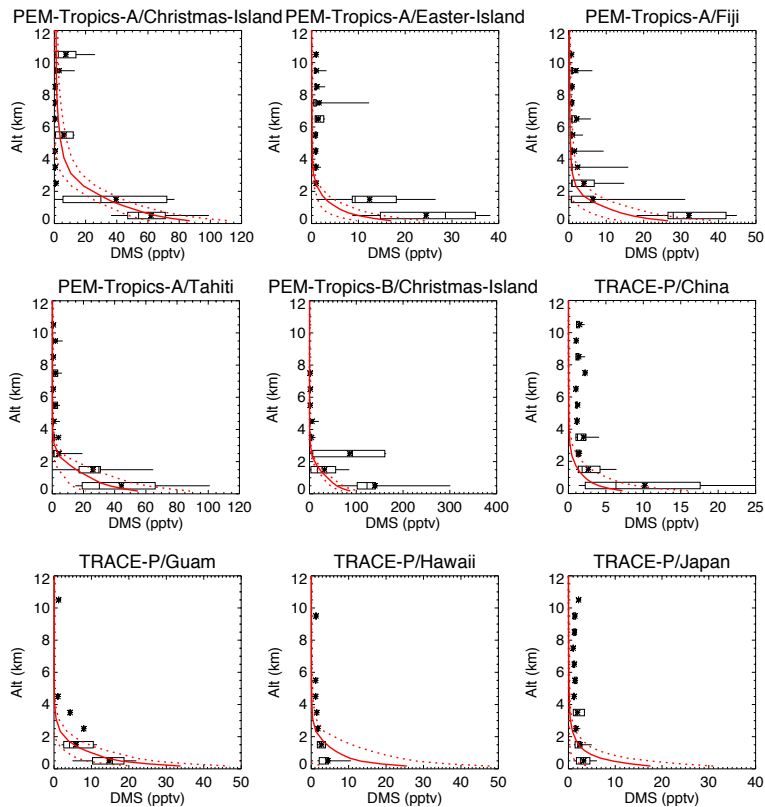


**Fig. 7.** DMS vertical profiles over the Pacific Ocean. Observations are from PEM-Tropics A (September–October, 1996), PEM-Tropics B (March–April, 1999), and TRACE-P (February–April, 2001) (Emmons et al., 2000). Model results (red lines) are monthly mean, and averaged over the observational domain (solid line: mean; dash lines:  $\pm$  one standard deviation). For the observed values (in black), the whiskers show 5th and 95th percentiles, the boxes show 25th and 75th percentiles, and the star symbols and thicker vertical lines inside the boxes show mean and median.

[Title Page](#)

[Abstract](#)

[Introduction](#)

[Conclusions](#)

[References](#)

[Tables](#)

[Figures](#)

[⏪](#)

[⏩](#)

[◀](#)

[▶](#)

[Back](#)

[Close](#)

[Full Screen / Esc](#)

[Printer-friendly Version](#)

[Interactive Discussion](#)



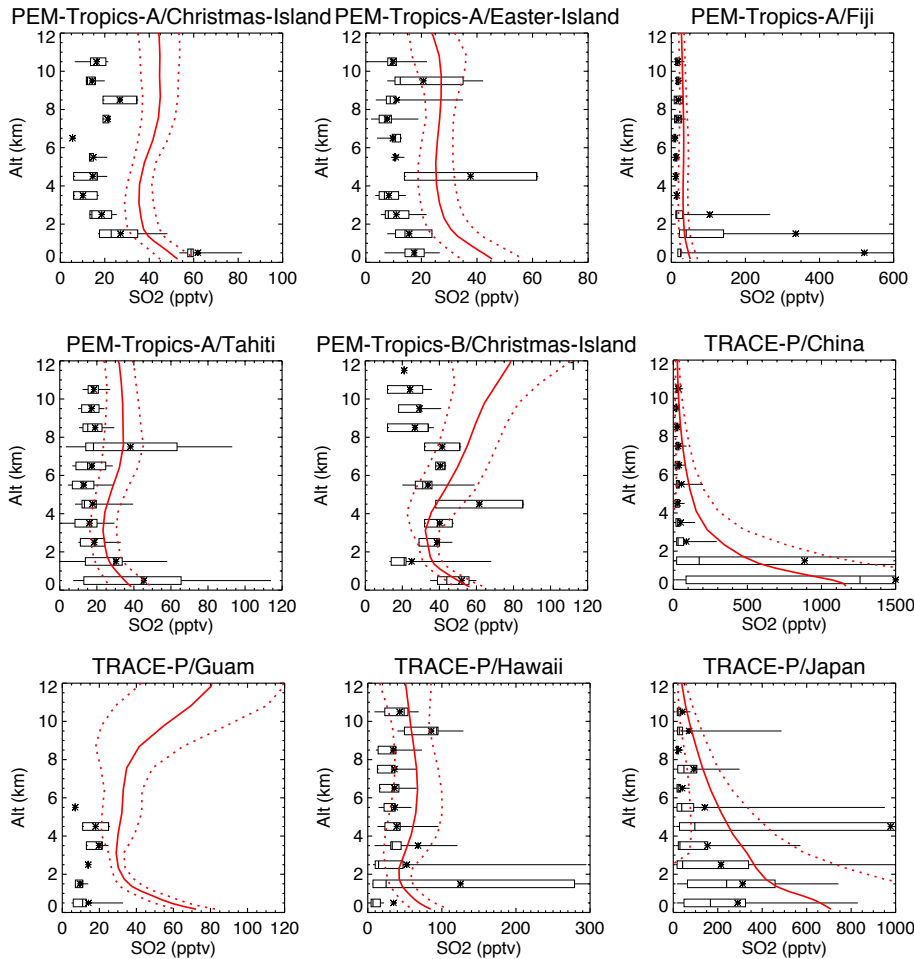
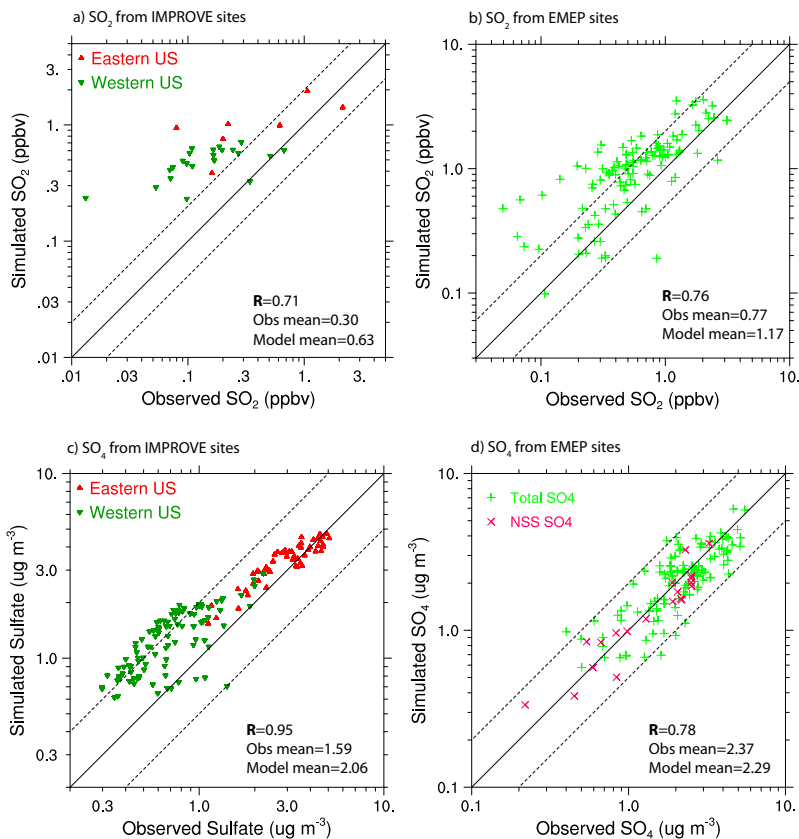


Fig. 8. The same as Fig. 7, but for SO<sub>2</sub> vertical profiles.

<a href="#">Title Page</a>	
<a href="#">Abstract</a>	<a href="#">Introduction</a>
<a href="#">Conclusions</a>	<a href="#">References</a>
<a href="#">Tables</a>	<a href="#">Figures</a>
<a href="#">◀</a>	<a href="#">▶</a>
<a href="#">◀</a>	<a href="#">▶</a>
<a href="#">Back</a>	<a href="#">Close</a>
<a href="#">Full Screen / Esc</a>	
<a href="#">Printer-friendly Version</a>	
<a href="#">Interactive Discussion</a>	





**Fig. 9.** Annual average simulated surface concentrations versus observations from the IMPROVE network and EMEP network: **(a)**  $\text{SO}_2$  concentrations at the IMPROVE sites; **(b)**  $\text{SO}_2$  concentrations at the EMEP sites; **(c)** sulfate concentrations at the IMPROVE sites; **(d)** sulfate concentrations at the EMEP sites. Model mean (“Model mean”), observational mean (“Obs mean”), and the correlation between model and observations (“R”) are shown in each panel.

[Title Page](#)  
[Abstract](#)   [Introduction](#)  
[Conclusions](#)   [References](#)  
[Tables](#)   [Figures](#)  
[◀](#)   [▶](#)  
[◀](#)   [▶](#)  
[Back](#)   [Close](#)  
[Full Screen / Esc](#)  
[Printer-friendly Version](#)  
[Interactive Discussion](#)



## A multi-scale aerosol climate model

M. Wang et al.

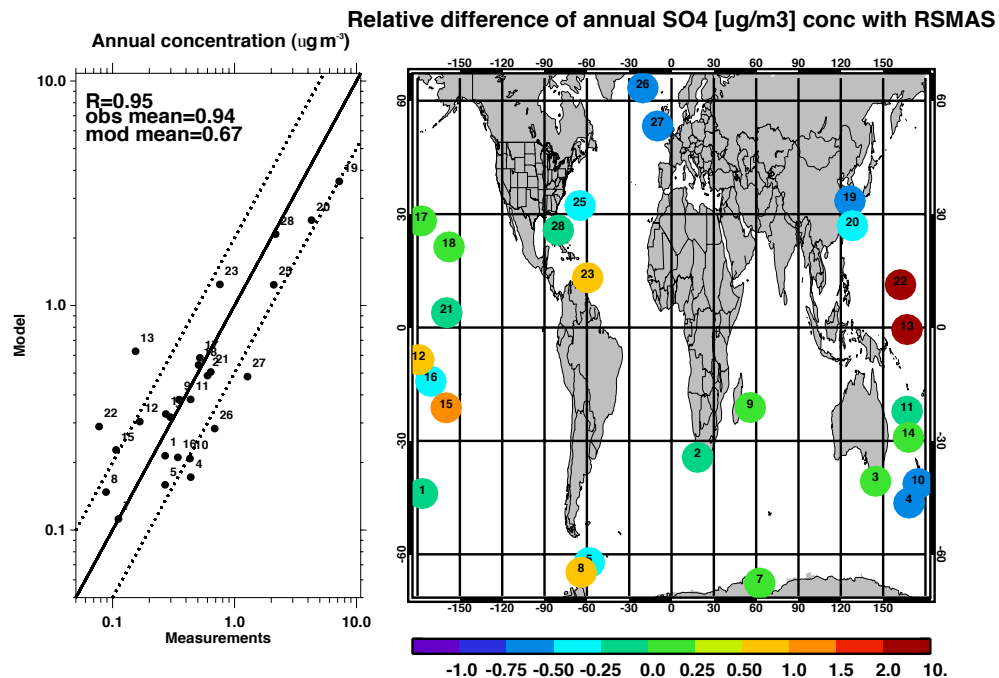


**Fig. 10.** Annual mean surface sulfate concentrations at the ocean network sites operated by the Rosenstiel School of Marine and Atmospheric Science (RSMAS) at the University of Miami (Arimoto et al., 1996; Prospero et al., 1989; Savoie et al., 1989, 1993). The left panel shows the scattering plot between the observations and the model. Model mean (“Mod mean”), observational mean (“Obs mean”), and the correlation between model and observations (“R”) are shown. The right panel shows the global map of individual sites, and the relative difference between the model and the observations:  $(\text{model}-\text{observations})/\text{observations}$ .

Title Page

Abstract

Introduction

Conclusions

References

Tables

Figures

◀

▶

◀

▶

Back

Close

Full Screen / Esc

Printer-friendly Version

Interactive Discussion



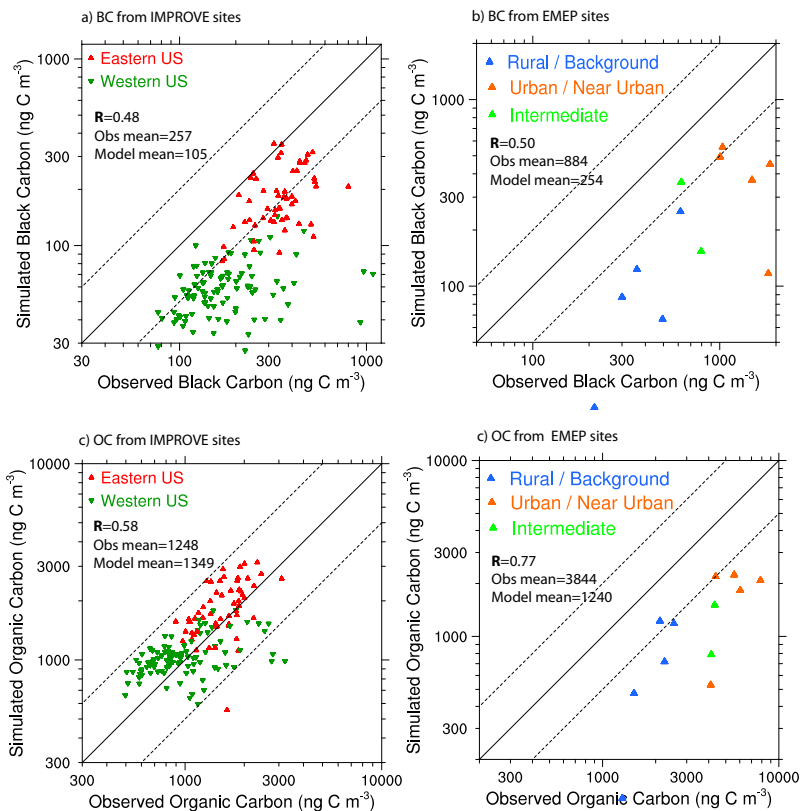


**Fig. 11.** Annual average simulated surface BC and OC concentrations versus observations from the IMPROVE network and EMEP network. **(a)** BC concentrations at the IMPROVE sites; **(b)** BC concentrations at the EMEP sites; **(c)** OC concentrations at the IMPROVE sites; **(d)** OC concentrations at the EMEP sites. Model mean (“Model mean”), observational mean (“Obs mean”), and the correlation between model and observations (“R”) are shown in each panel.

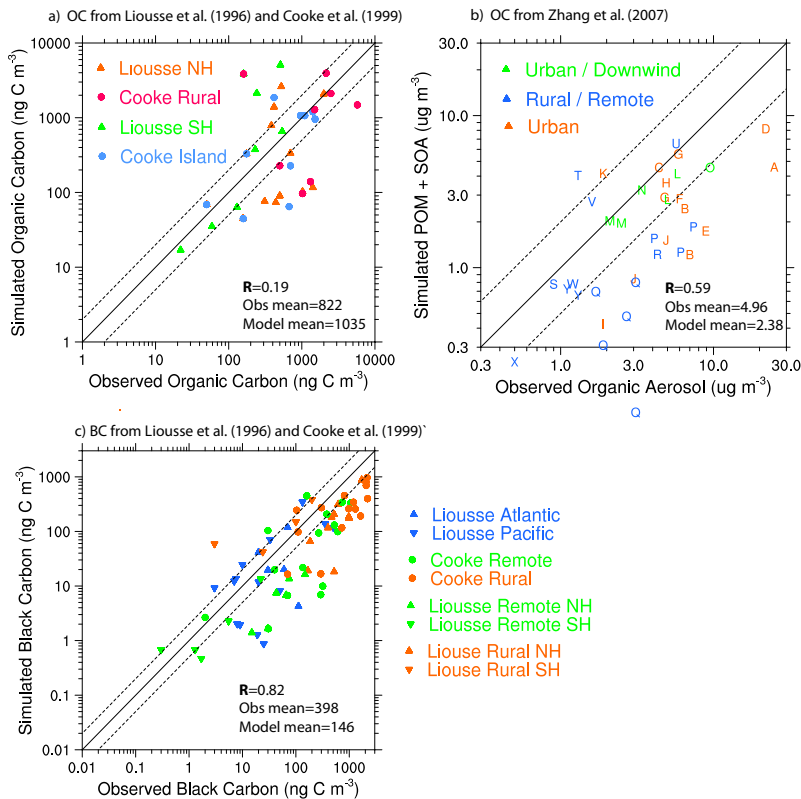


**Fig. 12.** Annual average simulated BC and OC concentrations versus observations from Lioussé et al. (1996), Cooke et al. (1999), and Zhang et al. (2007): **(a)** OC concentrations from Lioussé et al. (1996) and Cooke et al. (1999); **(b)** OC concentrations from Zhang et al. (2007); **(c)** BC concentrations from Lioussé et al. (1996) and Cooke et al. (1999). Model mean (“Model mean”), observational mean (“Obs mean”), and the correlation between model and observations (“R”) are shown in each panel.

A multi-scale aerosol climate model

M. Wang et al.

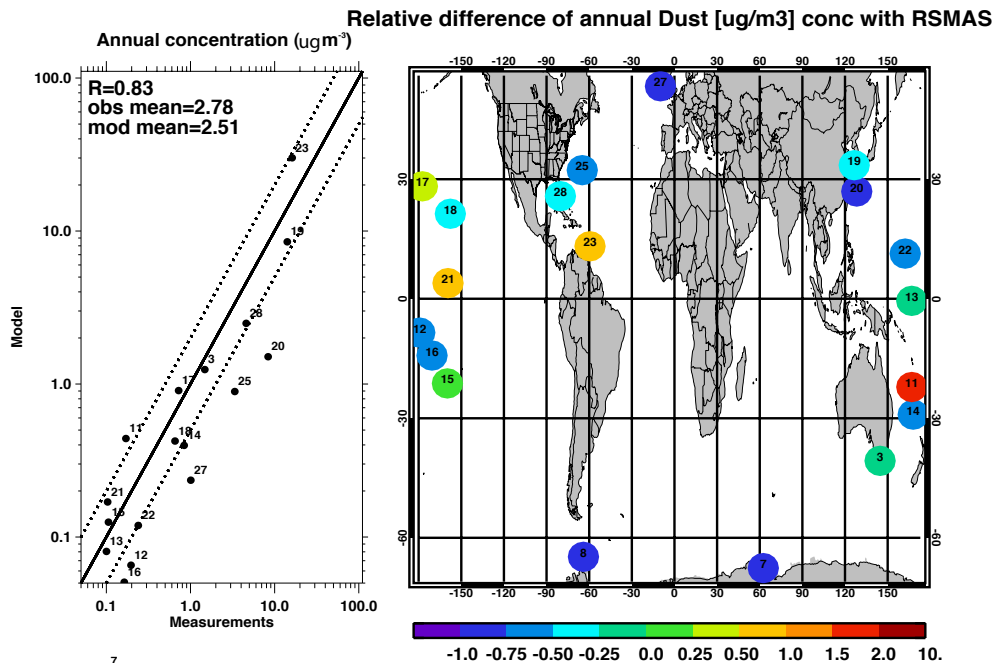


Fig. 13. The same as Fig. 10, but for dust.

Discussion Paper | Discussion Paper | Discussion Paper | Discussion Paper | Discussion Paper

Title Page

Abstract

Introduction

Conclusions

References

Tables

Figures

◀

▶

◀

▶

Back

Close

Full Screen / Esc

Printer-friendly Version

Interactive Discussion



A multi-scale aerosol climate model

M. Wang et al.

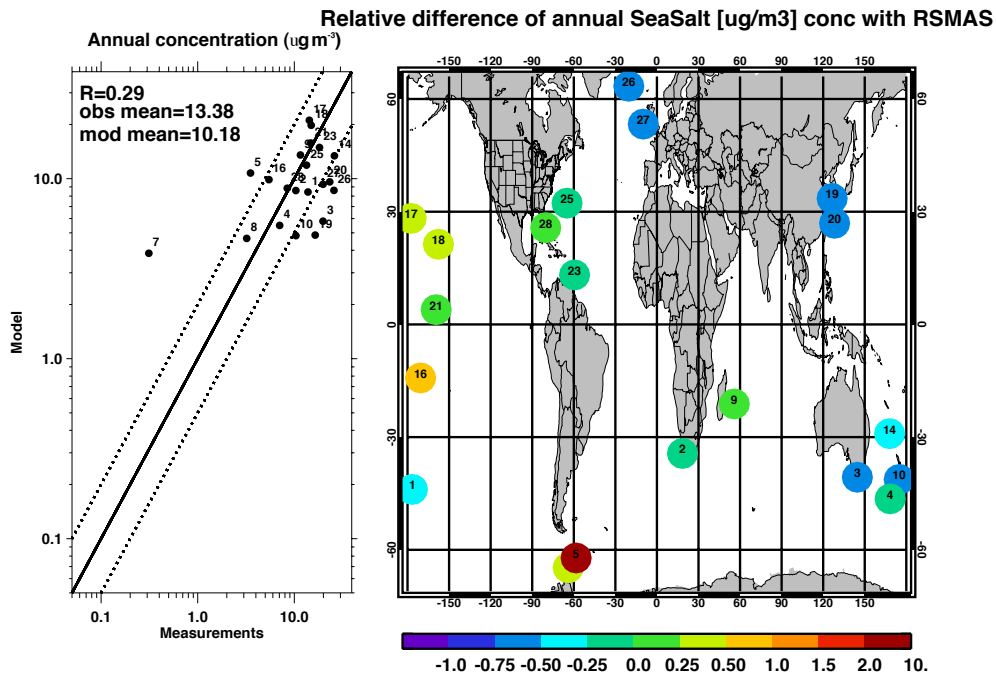


Fig. 14. The same as Fig. 10, but for sea salt.

Discussion Paper | Discussion Paper | Discussion Paper | Discussion Paper | Discussion Paper

Title Page

Abstract

Introduction

Conclusions

References

Tables

Figures

◀

▶

◀

▶

Back

Close

Full Screen / Esc

Printer-friendly Version

Interactive Discussion



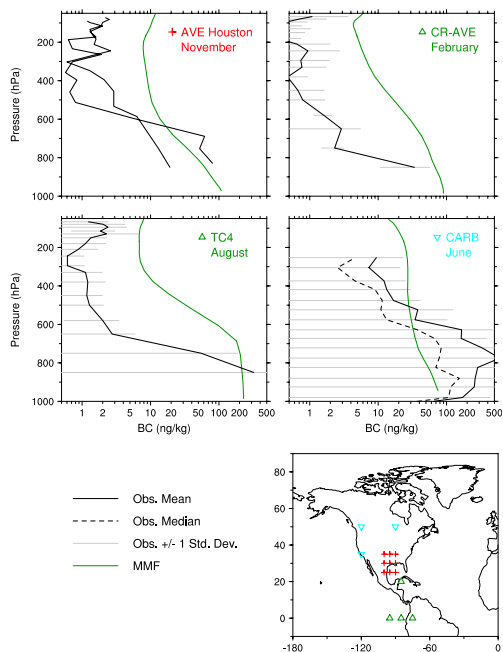


**Fig. 15.** BC vertical profiles in the tropics and middle latitudes over 4 different campaigns (AVE Houston: NASA Houston Aura Validation Experiment; CR-AVE: NASA Costa Rica Aura Validation Experiment; TC4: Tropical Composition, Cloud and Climate Coupling; CARB: NASA initiative in collaboration with California Air Resources Board). Model profiles are averaged over the points in the map. Observations are average for the respective campaigns and are measured by three different groups: the NASA group (Schwarz et al., 2006) for AVE-Houston, CR-AVE, and TC4; the University of Tokyo group (Moteki and Kondo, 2007; Moteki et al., 2007) for CARB; and the University of Hawaii group (Clarke et al., 2007; Howell et al., 2006; McNaughton et al., 2009; Shinozuka et al., 2007) for CARB. The Houston campaign has two profiles measured two different days. See Table 7 in Koch et al. (2009) for flight details.

Title Page

Abstract Introduction

Conclusions References

Tables Figures

◀ ▶

◀ ▶

Back Close

Full Screen / Esc

Printer-friendly Version

Interactive Discussion



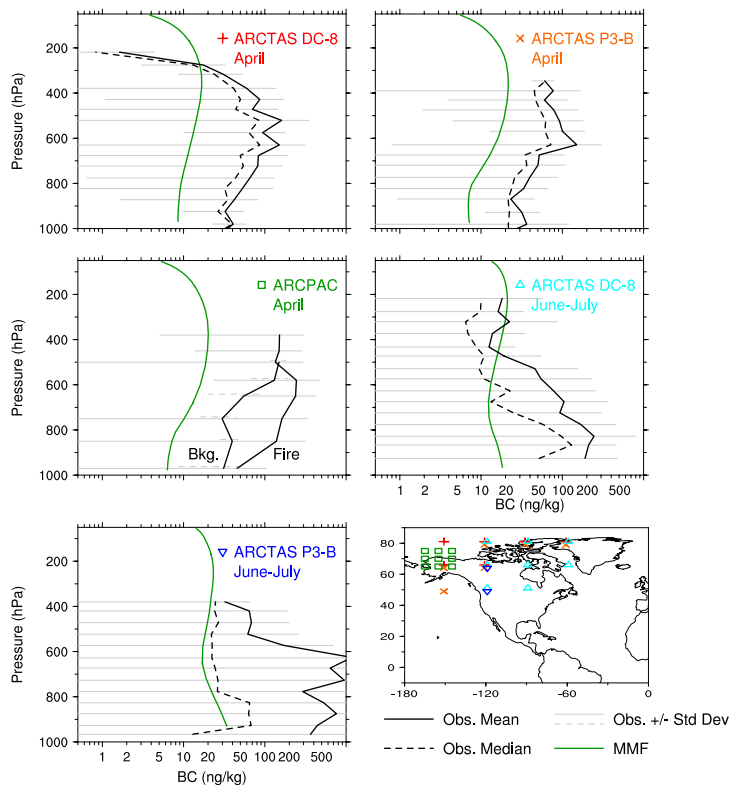


**Fig. 16.** The same as Fig. 15, but for BC vertical profiles in the high latitudes over two campaigns (ARCTAS: NASA Arctic Research of the Composition of the Troposphere from Aircraft and Satellite; ARCPAC: NOAA Aerosol, Radiation, and Cloud Processes affecting Arctic Climate). Observations are average for the respective campaigns, and are measured by three different groups: the NASA group for ARCPAC; the University of Tokyo group for ARCTAS; and the University of Hawaii group for ARCTAS. See Table 7 in Koch et al. (2009) for flight details.

[Title Page](#)

[Abstract](#)

[Introduction](#)

[Conclusions](#)

[References](#)

[Tables](#)

[Figures](#)

[◀](#)

[▶](#)

[◀](#)

[▶](#)

[Back](#)

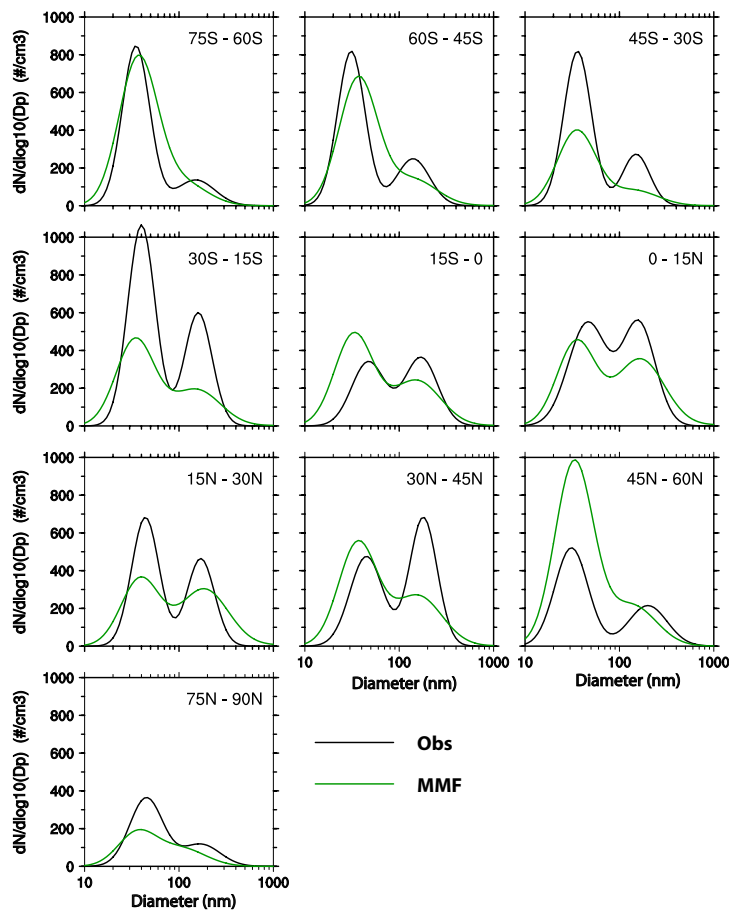
[Close](#)

[Full Screen / Esc](#)

[Printer-friendly Version](#)

[Interactive Discussion](#)

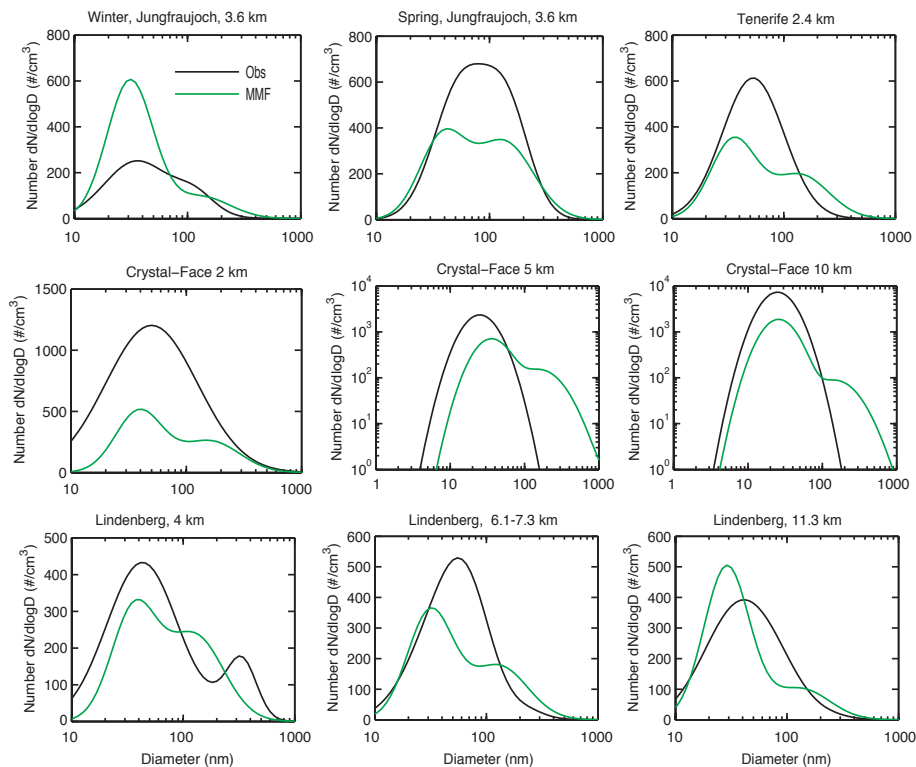




**Fig. 17.** Aerosol size distribution in the marine boundary layer. Observations (Obs) are from Heintzenberg et al. (2000).

[Title Page](#)  
[Abstract](#)   [Introduction](#)  
[Conclusions](#)   [References](#)  
[Tables](#)   [Figures](#)  
⏪   ⏩  
◀   ▶  
[Back](#)   [Close](#)  
[Full Screen / Esc](#)  
[Printer-friendly Version](#)  
[Interactive Discussion](#)



[Title Page](#)[Abstract](#)[Introduction](#)[Conclusions](#)[References](#)[Tables](#)[Figures](#)[Back](#)[Close](#)[Full Screen / Esc](#)[Printer-friendly Version](#)[Interactive Discussion](#)

**Fig. 18.** Aerosol size distributions in the free troposphere. Observations (Obs) are from Putaud et al. (2003) (Jungfraujoch), Raes et al. (2000) (Tenerife), Fridland et al. (2004) (CRYSTAL-FACE, Florida, US), and Petzold et al. (2002) (LACE8, Lindenberg, Germany).

Observed (INCA Campaigns) and Model Aerosol Number Profiles

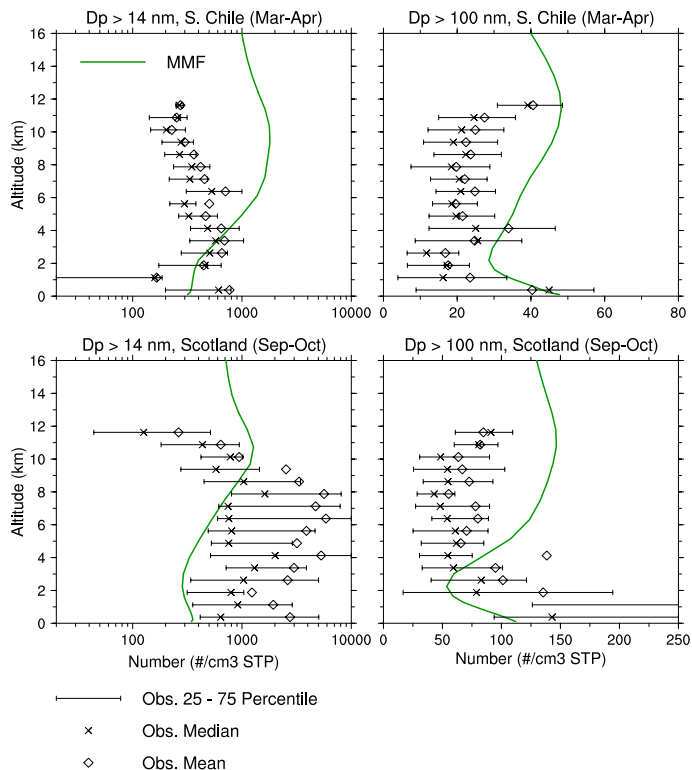


**Fig. 19.** Vertical profiles of the number concentration of (left) Aitken mode particles (diameter >14 nm) and (right) accumulation mode particles (diameter >100 nm) (top) over Punta Arenas, Chile, in March/April and (bottom) over Prestwick, Scotland, in September/October. Observations are from Minikin et al. (2003): median (star), 25 and 75 percentiles (left end and right end of error bars). Model results are averaged over 60°–50° S, 70°–85° W for Chile, and over 50°–60° N, 10° W–5° E for Scotland.

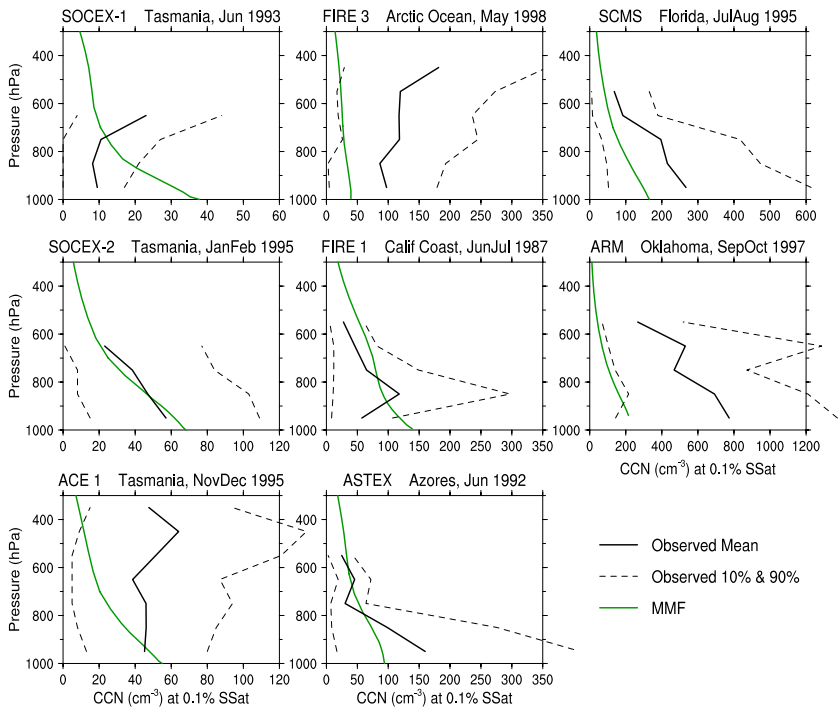


**Fig. 20.** Simulated vertical profiles of CCN concentrations at 0.1% supersaturation are compared with observations during each of eight field experiments (SOCEX-1, Tasmania, June, 1993; FIRE 3, Arctic Ocean, May, 1998; SCMS, Florida, July/August, 1995; SOCEX-2, Tasmania, January/February, 1995; FIRE-1, California Coast, June/July, 1987; ARM, Oklahoma, September/October, 1997; ACE1, Tasmanian, November/December, 1995; ASTEX, Azores, June, 1992) (see Table 1 in Ghan et al., 2001, for more details about each experiment). Model results are from monthly data, and shown in green line. Mean (solid black), 10 percentile and 90 percentile (dash lines) are shown for observations.

[Title Page](#)

[Abstract](#)   [Introduction](#)

[Conclusions](#)   [References](#)

[Tables](#)   [Figures](#)

[◀](#)   [▶](#)

[◀](#)   [▶](#)

[Back](#)   [Close](#)

[Full Screen / Esc](#)

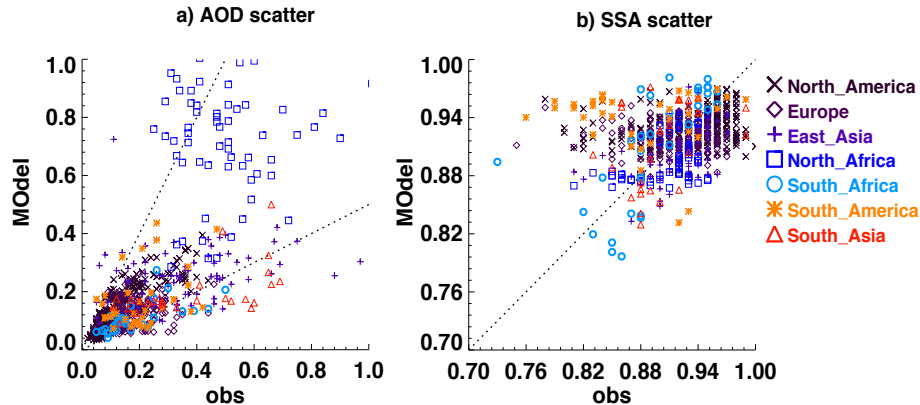
[Printer-friendly Version](#)

[Interactive Discussion](#)



## A multi-scale aerosol climate model

M. Wang et al.

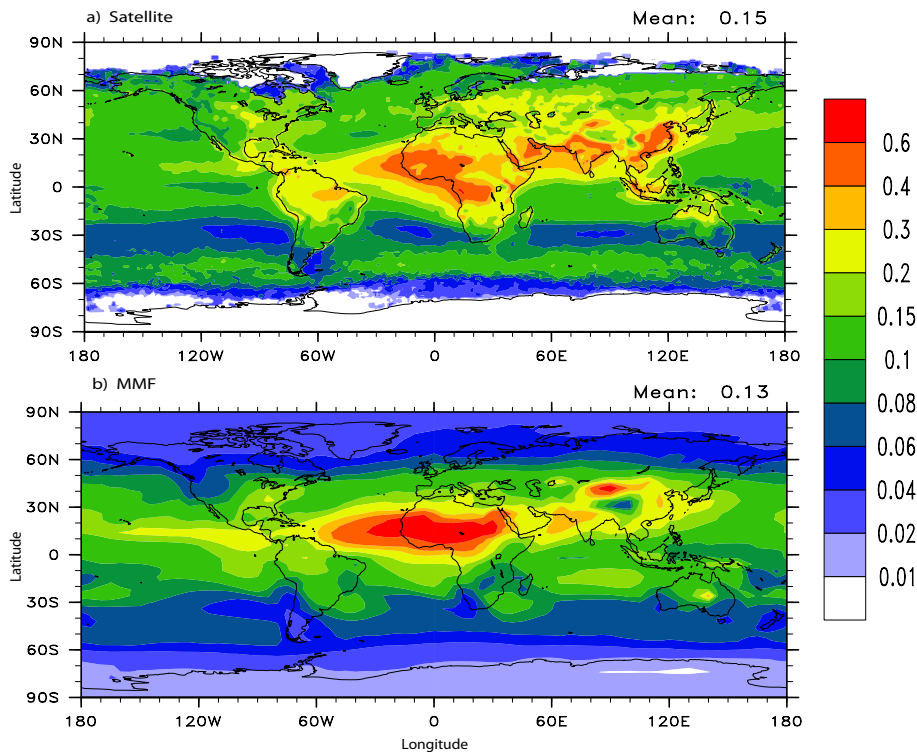


**Fig. 21.** Scatter plots of simulated monthly AOD and SSA in comparison with AERONET data. Results from several different regions (North America, Europe, East Asia, North Africa, South Africa, South America, and South Asia) are represented by 7 different colours and marks. The upper and lower dash lines in **(a)** are 2:1 and 1:2, respectively. The dash line in **(b)** is 1:1.

[Title Page](#)
[Abstract](#)
[Introduction](#)
[Conclusions](#)
[References](#)
[Tables](#)
[Figures](#)
[⏪](#)
[⏩](#)
[◀](#)
[▶](#)
[Back](#)
[Close](#)
[Full Screen / Esc](#)
[Printer-friendly Version](#)
[Interactive Discussion](#)


**A multi-scale aerosol  
climate model**

M. Wang et al.

[Title Page](#)[Abstract](#)[Introduction](#)[Conclusions](#)[References](#)[Tables](#)[Figures](#)[⏪](#)[⏩](#)[◀](#)[▶](#)[Back](#)[Close](#)[Full Screen / Esc](#)[Printer-friendly Version](#)[Interactive Discussion](#)

**Fig. 22.** Global annual-averaged AOD in the MMF model (a), and a satellite AOD retrieval composite (Kinne et al., 2006) (b).